Title
TOTAL CROSS SECTION OF K- MESONS ON NUCLEONS IN THE MOMENTUM REGION 630 Mev/c TO 1100 Mev/c.

Author
Maung, Maung Tin.

Publication Date
1962-03-15

UCRL 10125

University of California

Ernest O. Lawrence Radiation Laboratory

TOTAL CROSS SECTION OF K^- MESONS ON NUCLEONS IN THE MOMENTUM REGION 630 Mev/c TO 1100 Mev/c

Berkeley, California

DISCLAIMER

Research and Development

UCRL-10125
UC-34 Physics
TID-4500 (17th Ed.)

UNIVERSITY OF CALIFORNIA
Lawrence Radiation Laboratory
Berkeley, California

Contract No. W-7405-eng-48

TOTAL CROSS SECTION OF K^- MESONS ON NUCLEONS IN THE MOMENTUM REGION 630 Mev/c TO 1100 Mev/c

Maung Tin Maung

(Ph. D. Thesis)

March 15, 1962

TOTAL CROSS SECTION OF K^- MESONS ON NUCLEONS IN THE MOMENTUM REGION 630 Mev/c TO 1100 Mev/c

Contents

Abstract v

I. Introduction 1

II. Experimental Method 3

III. Beam and Experimental Equipment

A. The K^- Beam 5

B. The Hydrogen-Deuterium Target 7

C. The Cerenkov Counters for Selecting K^- Beam . . 10

IV. Electronics 15

V. Experimental Procedure 18

A. General Description 18

B. Identification of K^- Mesons 18

C. Time-of-Flight Measurements 21

D. Measurement of Momentum 26

VI. The Yield of K^- Mesons 31

VII. Calculation of the Total Cross Sections 34

A. Accidental Counts and Rate Sensitivity 37

B. Forward Scattering 46

C. Decays in Flight 47

D. Multiple Coulomb Scattering and Beam Divergences 49

E. Light-Particle Contamination 51

VIII. K^--Neutron Total Cross Sections 58

IX. Uncertainties in the Calculated Cross Sections 60

X. Results 63

Contents (continued)

XI. Discussion of Results 64

Acknowledgments 68

Appendices

A. Raw Data Tables 69

B. Decay-in-Flight Corrections 71

C. Multiple Coulomb Scattering and Beam Divergence Corrections . . . 76

References 80

TOTAL CROSS SECTION OF K^- MESONS ON NUCLEONS IN THE MOMENTUM REGION 630 Mev/c TO 1100 Mev/c

Maung Tin Maung

Lawrence Radiation Laboratory
University of California
Berkeley, California

April 15, 1962

ABSTRACT

The total cross sections of K^- mesons in hydrogen and deuterium were measured over the momentum range 630 to 1100 Mev/c. The K^--n total cross sections were obtained from the hydrogen and deuterium data. These cross sections, with an accuracy of better than 5% were measured at the Berkeley Bevatron by counter techniques. Two high-resolution velocity-selecting Cerenkov counters were used to select the K^- mesons. The momentum of the K^- beam was measured with a counter telescope and an analyzing magnet. The K^--p and K^--d cross sections were measured at nine and five representative momenta respectively.

A well-defined resonance appears in the K^--p total cross section at about 1050 Mev/c K^- momentum(laboratory system). The neutron cross sections do not have enough statistical accuracy to enable us to infer any structure.

I. INTRODUCTION

Recently, a great deal of attention has been focused on the study of the K meson–nucleon interaction. The total cross sections of both K^+ and K^- mesons on nucleons are of great importance, in that they allow us to determine the nature of the K meson–nucleon forces. These cross sections have been previously measured at several energies by means of bubble chambers, counters, and nuclear emulsions.[1-7] Most of the published bubble chamber and emulsion works have rather large errors and are too widely spaced to allow more than the general trend of the cross section with energy to be inferred. At low energies, these measurements show that for momenta below a few hundred Mev/c, the K^--p cross section roughly follows a 1/v law. This dependence has been described by Dalitz and Tuan, who assumed a dominantly s-wave interaction.[8] Although there are some data on the absorption process of K^- mesons on neutrons, there is no information on the total cross section at these low energies.

In a recent experiment, Cook et al made a study of the behavior of the K^- meson cross sections on protons and neutrons in the momentum region 1 to 4 Bev/c.[5] They obtained evidence of the existence of structure in the K^--p total cross section, in particular the difference in the behavior of T = 0 and T = 1 K^--nucleon cross sections. Bastien et al. used a hydrogen bubble chamber to measure the K^--p total cross sections up to 800 Mev/c.[6] There seemed to be a disagreement between their results and the counter experiment of Cook et al.[5] The object of this experiment was therefore to measure the K^--p and K^--n total cross sections near 1 Bev/c, that is, at the lower end of the region studied by Cook et al,[5] but with considerably higher momentum resolution and at more closely spaced intervals; and also to explore further the missing region between the high-energy counter and the low-energy bubble chamber and emulsion observations. Thus, between the momenta 630 and 1100 Mev/c, K^--p and K^--n total cross sections were measured at nine and five values of incident momenta respectively. The momentum width chosen (between 1 and 2%) was about one-fifth as large as that in

the experiment of Cook et al.,[5] and although the counting rate was correspondingly smaller, it was possible thereby to study finer details of the structure in the total cross sections.

The techniques used in this experiment are described in Section II. Data analysis and corrections applied are described in Section VII. In Section XI, discussions are given for the different possible processes which may give rise to the observed resonance in the K^--p total cross section at about 1050 Mev/c.

II. EXPERIMENTAL METHOD

The general method for measuring the cross sections was that for a transmission experiment. The attenuation of K^- mesons by hydrogen and deuterium was measured by comparing the difference in attenuation by a full and an empty target. This method automatically corrects for such spurious effects as counter inefficiency, or attenuation by empty target assembly and other material in the beam. The basic arrangement is shown in Fig. 1.

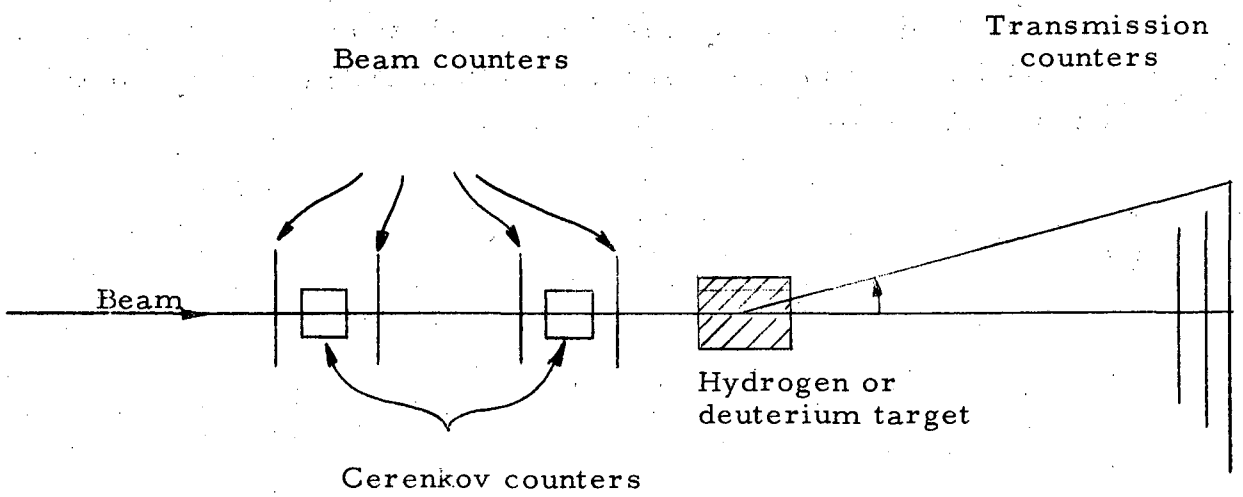

Fig. 1.

If T_E and T_F are the transmission factors for the empty and full target respectively, the total cross section is given by

$$\sigma = \frac{1}{nL} \ln \frac{T_E}{T_F},$$

where n is the number of target nuclei per cm^3, and L is the length of the target in c m. Under the operating pressure and temperature of the target, n represents the difference in atomic concentration between gas in the empty target and the liquid in full target. The above expression gives the exact total cross section under the ideal situation of a good geometry. In most cases, since the transmission counter subtends a finite solid angle, a transmission counter measures an apparent total cross section that is equal to the total cross section, reduced by an amount equal to the integral of the angular distribution of all charged particles resulting from scattering events from zero to the half-angle subtended by the counter. To be able to correct for this effect, we used three separate transmission counters in the experiment, subtending different solid angles at the target.

III. BEAM AND EXPERIMENTAL EQUIPMENT

A. The K^- Beam

The arrangement of counters and magnets used to obtain a variable-momentum K^--meson beam of narrow momentum width is shown in Fig. 2. The primary target was of stainless steel, 6×1/2×1/4 in., located in the magnet gap of the Bevatron. Negative particles produced within about 6 deg to the direction of the circulating internal proton beam entered the channel after passing through a 0.020-in. aluminum window in the vacuum tank at the beginning of the west straight section of the Bevatron. The first bending magnet M_1, a 13×24-in. and 6-in.-gap C magnet, was used to correct for variation in the apparent target position with selected secondary beam momentum. For particles at the center of the momentum interval accepted, a horizontal image of the internal Bevatron target was formed at the center of the quadrupole field lens S by the 8-in.-diam, 16×16-in. quadrupole doublet Q. The field lens was a 4-in.-diam 16-in.-long quadrupole singlet. A vertical image of the target was formed at the position of the transmission counters T_1, T_2, and T_3 by the combination of Q and S. The 18×36-in. and 8-in.-gap H magnet M_2, set for symmetric entry and exit, primarily defined the operating momentum of the system. The main function of the bending magnet M_3, also a 13×24-in. and 6-in.-gap C magnet, was to remove degraded particles from the beam. A calibration of the operating momentum of the system was obtained by the floating-wire technique, with all three bending magnets in their final locations. A more precise value of the momentum and, in addition, the momentum spread, was obtained by using a 29×36-in. deflecting magnet, downstream from the apparatus, to analyze the unscattered beam (see Section V-D).

Four scintillation counters B_1, B_2, B_3, and B_4, all with 3×3-in. plastic scintillators 1/4 in. thick in the beam direction, defined the beam particles, as shown in Fig. 2. A fifth scintillation counter,

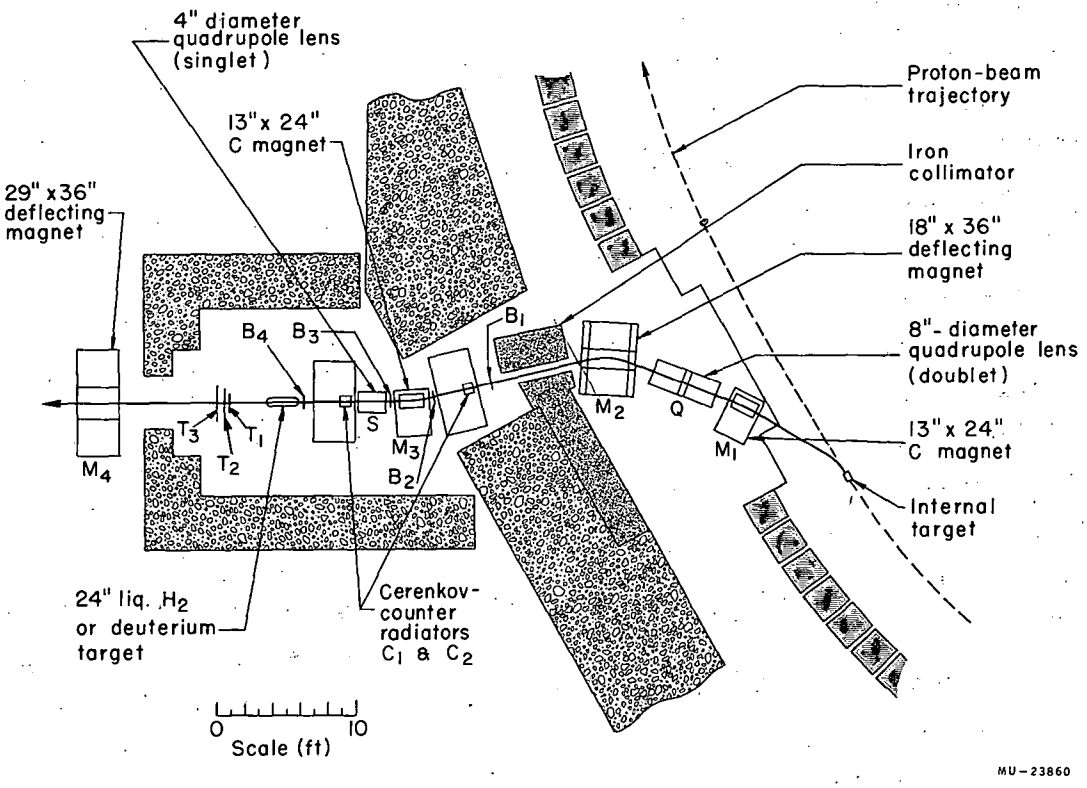

Fig. 2. Arrangement of K^- beam. M_1, M_2, and M_3 are bending magnets, Q is a quadrupole doublet and S is a quadrupole singlet lens. Scintillation counters B_1, B_2, B_3, and B_4 define the beam, and T_1, T_2, and T_3 measure the transmission.

called A, with a 3×3-in. hole at the center, was placed next to B_4 to act as an anticoincidence counter for the beam. Two velocity-selecting coincidence-anticoincidence Cerenkov counters C_1 and C_2 (see Fig. 5), with the two scintillation counter pairs, B_1-B_3 and B_2-B_4, together with the anticoincidence counter A, selected the K^- mesons in the beam and rejected π^- mesons, μ^- mesons, electrons, and antiprotons. The time delays between B_1 and B_3, and between B_2 and B_4, were respectively adjusted so that some velocity discrimination between K^- and π^- mesons was possible. This was more effective at the lower momenta than at the higher. At all operating momenta, antiprotons were rejected by this means.

B. The Hydrogen-Deuterium Target

Figure 3(A) shows a cut-away view of the target flask and the aluminum vacuum jacket. The target flask, made from 0.010-in. Mylar, was 24 in. long × 6 in. in diam, and was surrounded by a 0.002 in. aluminized Mylar heat shield. The aluminum jacket for the vacuum insulation had a 0.035-in. Mylar entrance window and a 0.032-in. aluminum exit dome as shown in the figure. Figure 3(B) is a schematic drawing showing all the essential components of the hydrogen-deuterium target.

During the hydrogen runs the lower reservoir (called the LD_2 reservoir in Fig. 3B, left of center in the diagram) was filled with liquid hydrogen, and the upper reservoir was kept empty. During the runs with deuterium, liquid deuterium was placed in the LD_2 reservoir, and the LH_2 reservoir was filled with liquid hydrogen. The liquid hydrogen in the upper reservoir served to condense the deuterium, which was maintained in a closed system. The deuterium system was kept at a slightly positive pressure by introducing helium gas into it. This allowed helium gas to escape from the system in case of a leak, rather than allowing air in which would contaminate the deuterium.

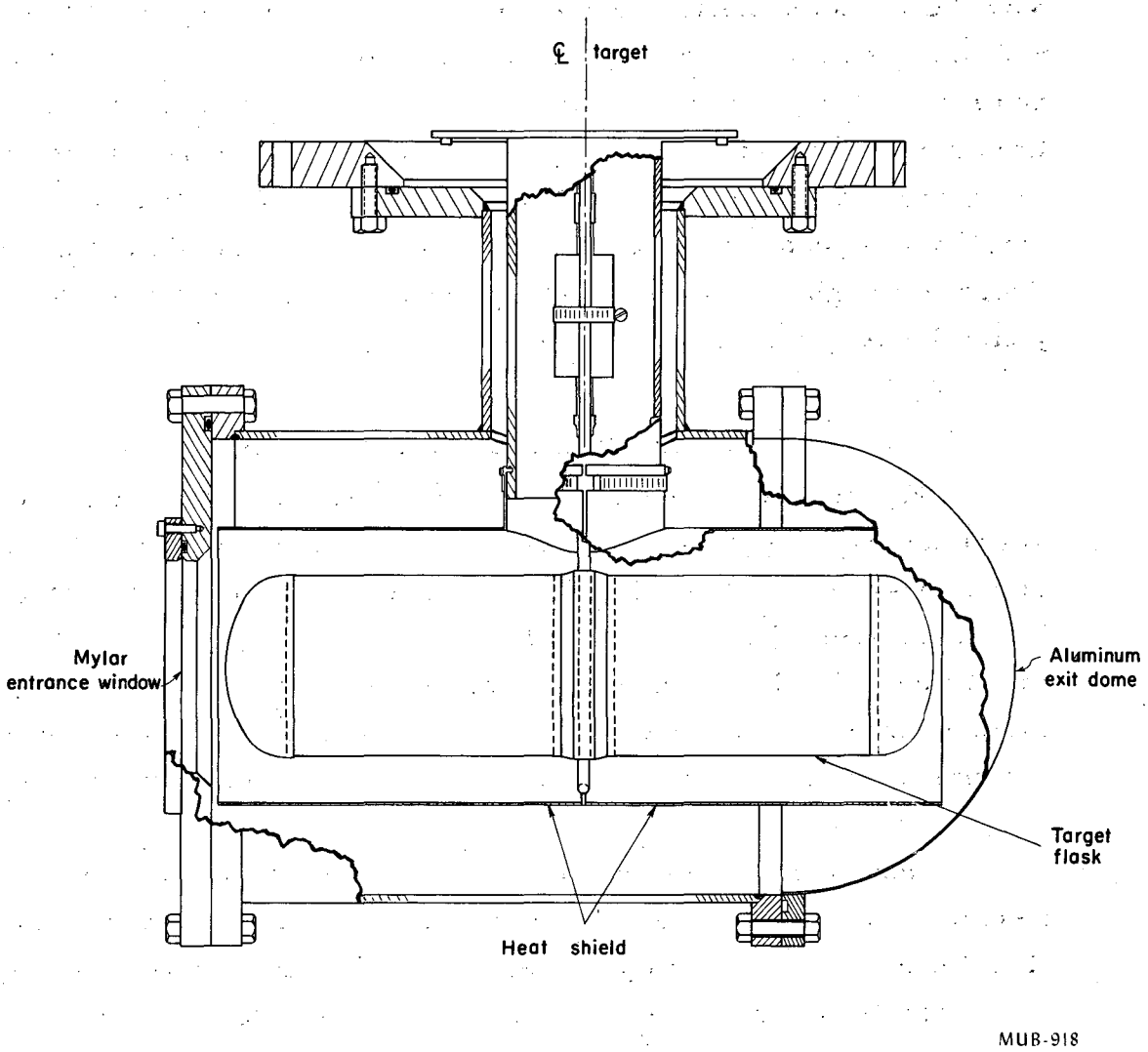

Fig. 3(A). Cutaway view of the target flask and the aluminum vacuum jacket.

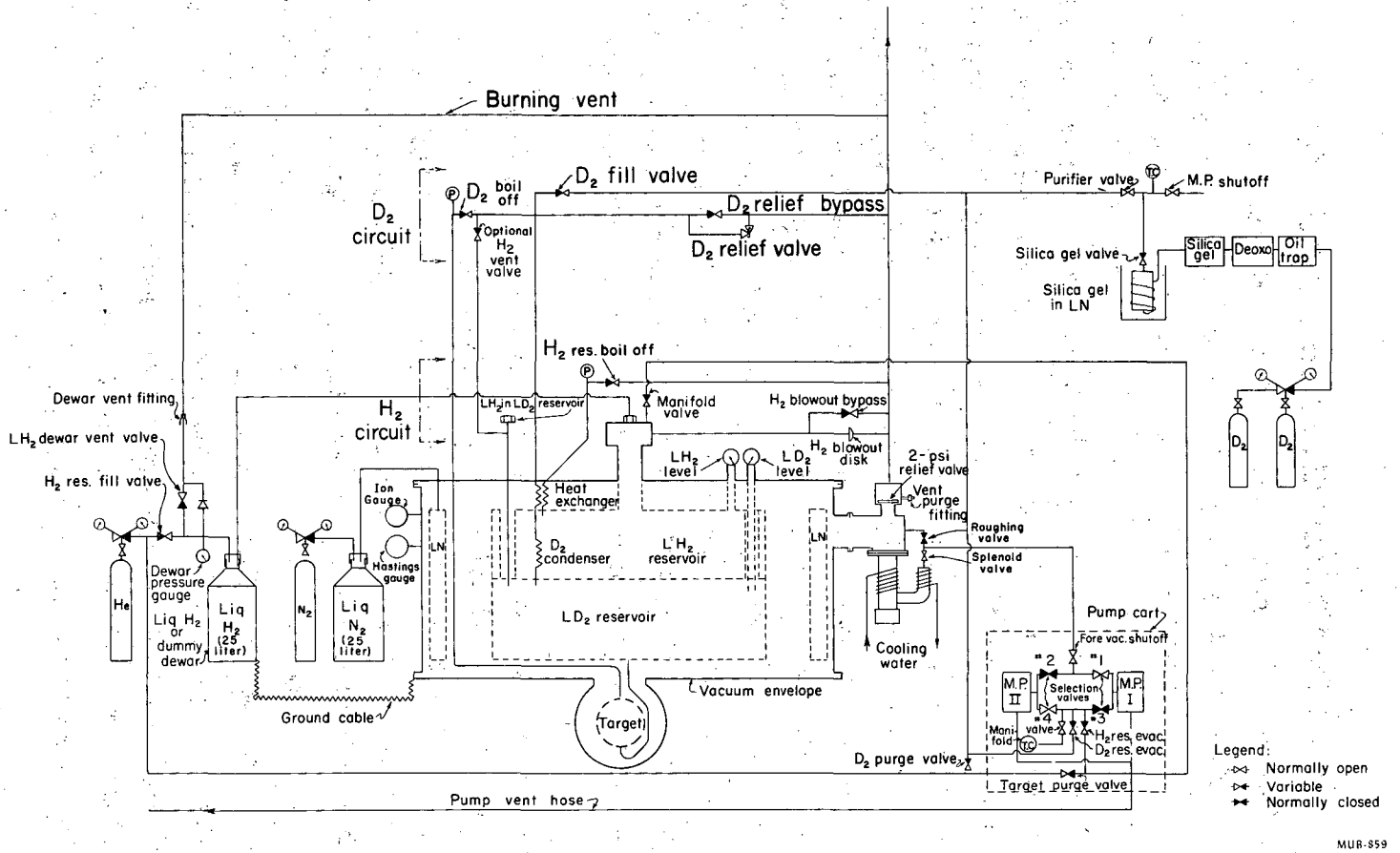

Fig. 3(B). Schematic drawing of the whole hydrogen-deuterium target system.

The liquid level in the reservoirs was monitored by means of Magnet-Helix level indicators, and the level in the target flask could be observed through the view ports.

C. The Cerenkov Counters for Selecting K^- Mesons

The Cerenkov counters are similar to the narrow-band velocity-selecting type described by Wiegand.[9] They are illustrated in Figs. 4(A through C). The two Cerenkov counters are almost identical except that in the second one, C_2, the light cones are inverted by placing a mirror downstream from the Cerenkov radiator (see Fig. 4C). It should be noted that these counters not only provide a "yes" signal when a K meson passes through, but also provide a "no" signal when a lighter particle traverses the radiator. Counter C_1 is located after the primary momentum-selecting magnet, M_2, while C_2 is placed after the singlet quadrupole field lens S. The Cerenkov radiators are right circular cylinders, 2 in. in diam $\times$ 2 in. thick, with axes parallel to the beam direction. The radiators have an 8-in. radius positive curvature on the exit face. For momenta from 600 to 800 Mev/c, a lucite radiator was employed (Fig. 4B). At higher momenta, the radiator was liquid Fluorochemical (FC-75) in a lucite container (Figs. 4A and C).

A particle of velocity β traveling parallel to the radiator axis produces a cone of Cerenkov light of half-angle θ_c given by $\cos\theta_c = 1/(n\beta)$, where n is the refractive index of the radiator. The light produced by K mesons of the correct momentum leaves the downstream end of the radiator and is deflected at this surface to a wider angle θ_r, owing to combined effects of refraction at the exit face and divergence because of the exit face curvature. This light is then transmitted by specular reflection down an aluminum light pipe to the photocathode of an RCA-7046 photomultiplier tube. Light leaving the radiator at angles greater than θ_r is prevented from entering this light pipe by a circular aluminum baffle. There are, at this angle, six such light pipes, and

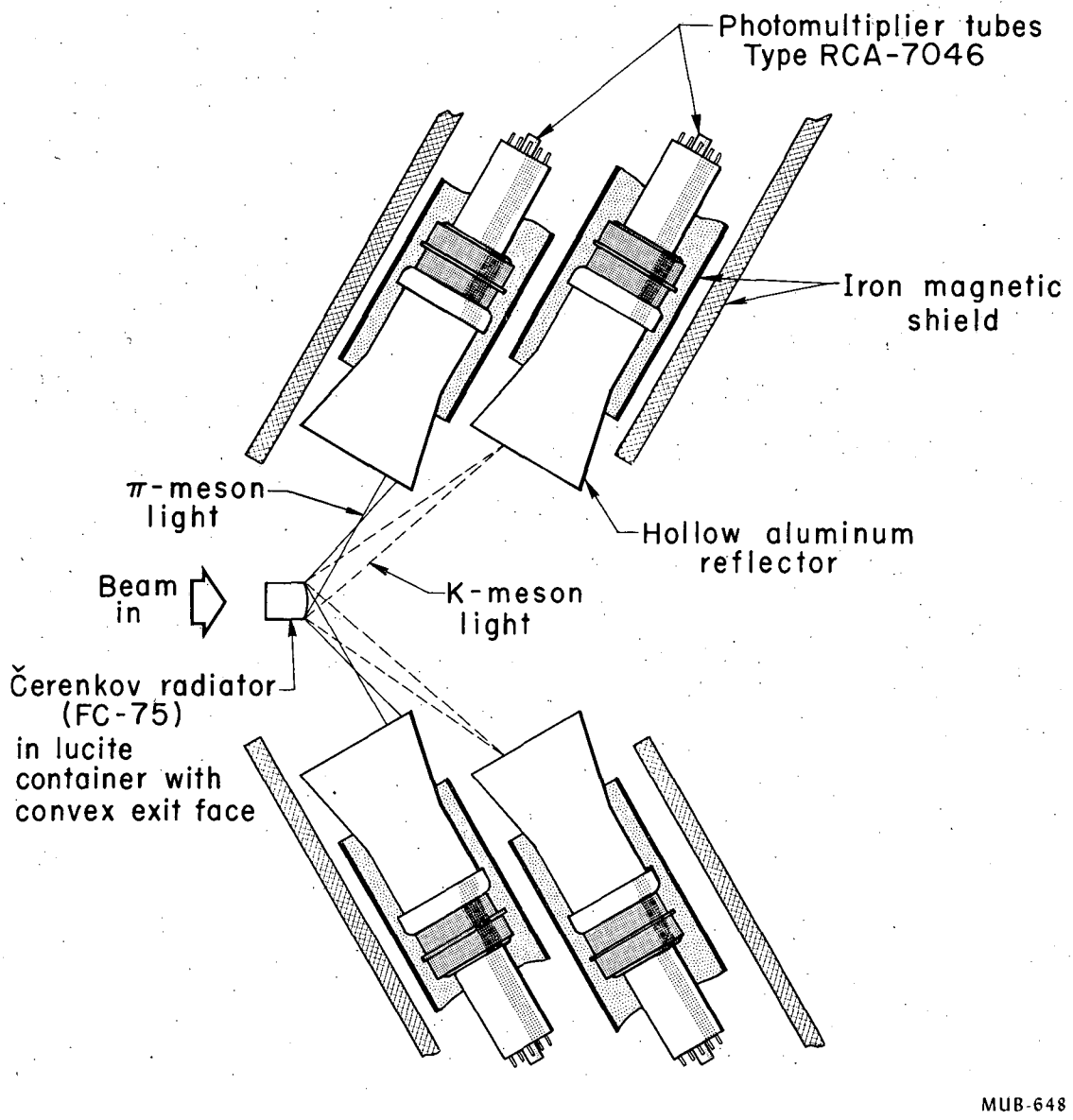

Fig. 4(A). Cerenkov counter operating mode I. Both K and π light leave the exit face of the Cerenkov radiator. The radiator used in this operating mode was liquid Fluorochemical (FC-75).

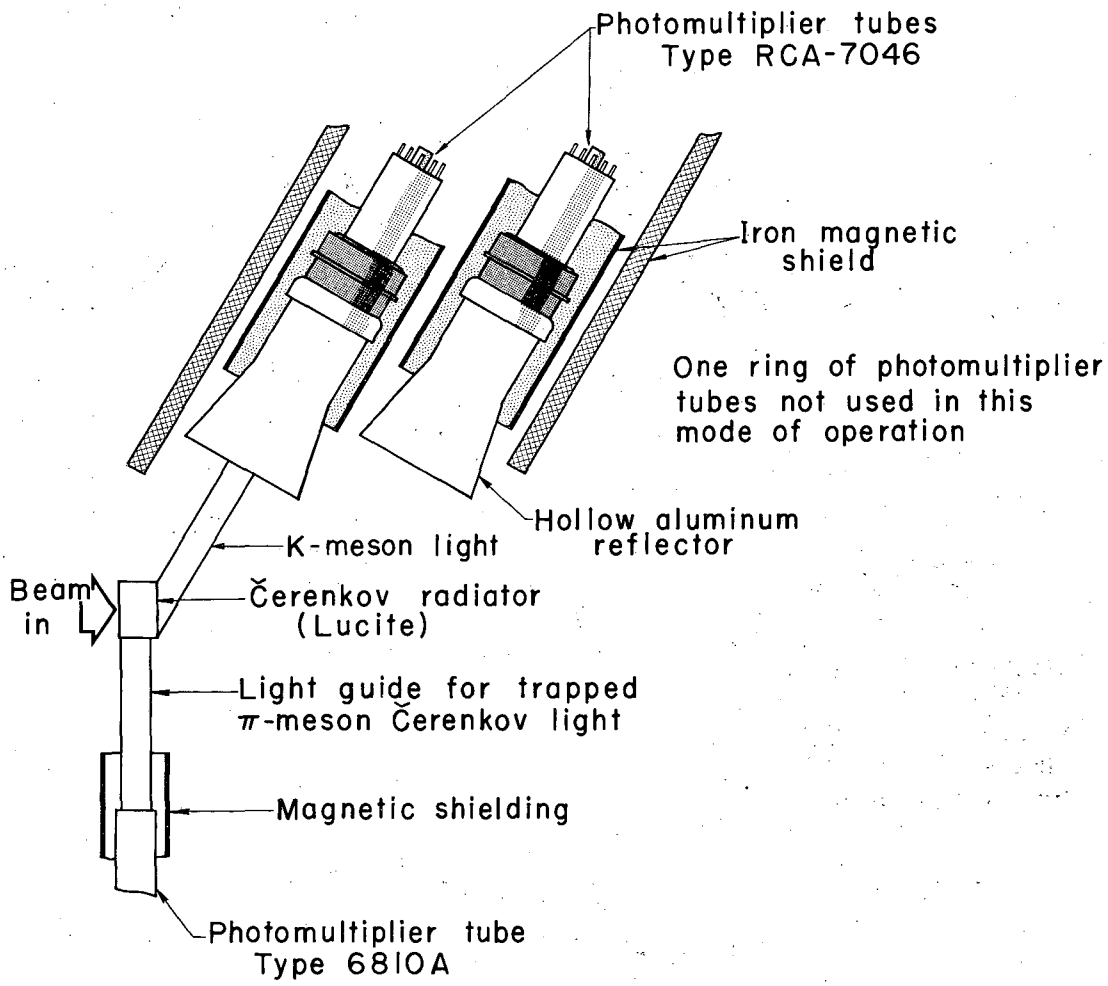

Fig. 4(B). Cerenkov counter operating-mode II. The lucite light pipe collects the π-light which is trapped in the radiator. A single RCA-6810A photomultiplier tube attached to this light pipe provides the anticoincidence signal.

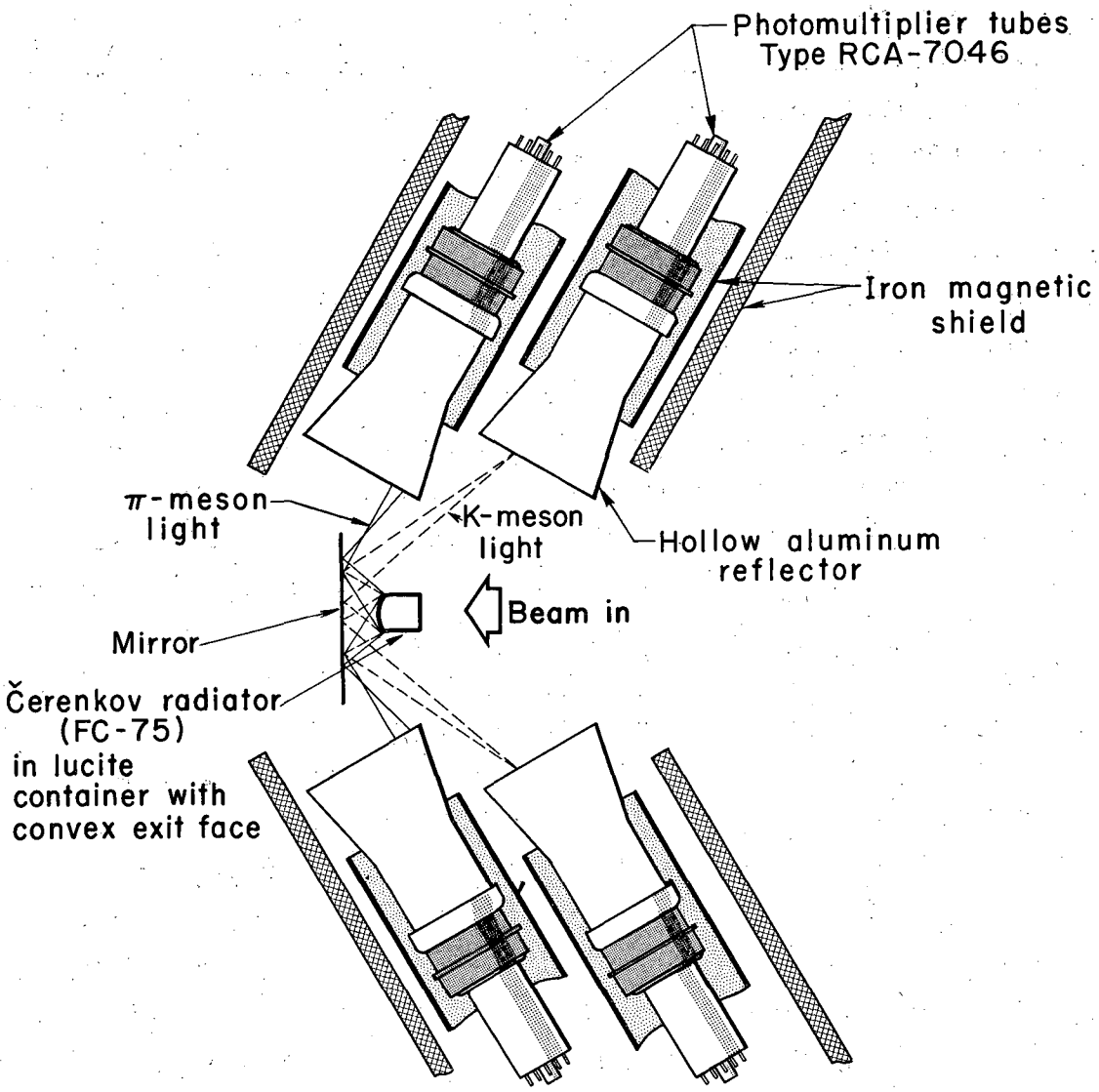

Fig. 4(C). Figure showing the mirror in Cerenkov counter C2 which inverted the light cones.

photomultipliers for each, placed in a ring about the beam axis. These six channels are divided into two groups of three each by adding together the signals from the alternate channels. A coincidence between signals from the two groups must be formed in order that a K meson be counted. Lighter particles produce Cerenkov light at a larger angle than a K meson of the same momentum. For momenta above 800 Mev/c, this light leaves the end window of the radiator at an angle greater than that for the K light and is collected by light pipes similar to those used to collect the K light. Again there are six light pipes with photomultipliers, placed in a ring about the beam axis. The entrance apertures of these light pipes are in such positions that they will intercept light leaving the radiator at angles larger than those corresponding to the K light. The anticoincidence signal is obtained by adding together the pulses from the six photomultipliers. In this way, a signal from any one of the six photomultipliers in a single counter unit can give an anticoincidence pulse which will reject the unwanted light particle. This mode of operation is illustrated in Fig. 4(A). For the momentum range from 600 to 800 Mev/c, the angle of the Cerenkov light produced by the light particles is such that it always strikes the exit face of the lucite radiator at an angle greater than the critical angle, and hence is trapped in the radiator. This light is collected by a single lucite light pipe in optical contact with one of the side walls of the radiator, and is transported to the photocathode of an RCA-6810A photomultiplier tube. The signal from this tube then provides the anticoincidence signal. Figure 4(B) illustrates this type of operation. The baffles and light pipes in the counter rings were designed to accept a beam divergence of not greater than ± 2 degrees. This also puts a limit on the accepted momentum band to about $\pm 5\%$, the velocity resolution being about $\pm 1.5\%$

IV. ELECTRONICS

A simplified block diagram of the basic electronics used in the experiment is shown in Fig. 5. Counters B_1, B_2, B_3, and B_4 are the beam counters, A is the beam anticoincidence counter, and C_1 and C_2 are the two Cerenkov counters. The transmission counters are denoted by T_1, T_2, and T_3. One final counter, TF, is the time-of-flight counter. All the electronic components used are standard Lawrence Radiation Laboratory equipment. The photomultiplier tubes used in the scintillation counters were all RCA-6810A tubes; the Cerenkov counters had twelve RCA-7046 photomultiplier tubes each.

As described earlier, each Cerenkov counter gave two "yes" signals and a "no" signal. They are denoted in Fig. 5 by C_1A, C_1B, $\overline{C}_1$, C_2A, C_2B, and $\overline{C}_2$. The signals from beam counters B_1 and B_3 were put in coincidence with C_1A and in anticoincidence with $\overline{C}_1$. Similarly, the signals from B_2 and B_4 were put in coincidence with C_2A and in anticoincidence with $\overline{C}_2$. The signals from each Cerenkov counter (C_1A, C_1B, and $\overline{C}_1$, etc.) were also put into a separate coincidence-anticoincidence unit. The coincidence circuits used were the fast 3-channel coincidence and anticoincidence units designed by Wenzel.[10] The outputs from two of the coincidence circuits, α and β, were put in coincidence in a separate fast coincidence circuit K, together with the signal from the beam anticoincidence counter A. Also, the output signals from coincidence circuits α, β, P_1, and P_2 were put in slow coincidence with the output of the K circuit in a multiple coincidence and anticoincidence circuit K'.[11] The K' output signal was taken as the final K^- meson signal. Finally, the output of K' was connected to a gated multichannel double-coincidence circuit that was gated by the output signal of the fast coincidence circuit K. The double-coincidence circuit gave an output signal every time a coincidence occurred between a K' signal and a signal from any of the transmission counters. It gave separate output signals for coincidence with individual transmission counters.

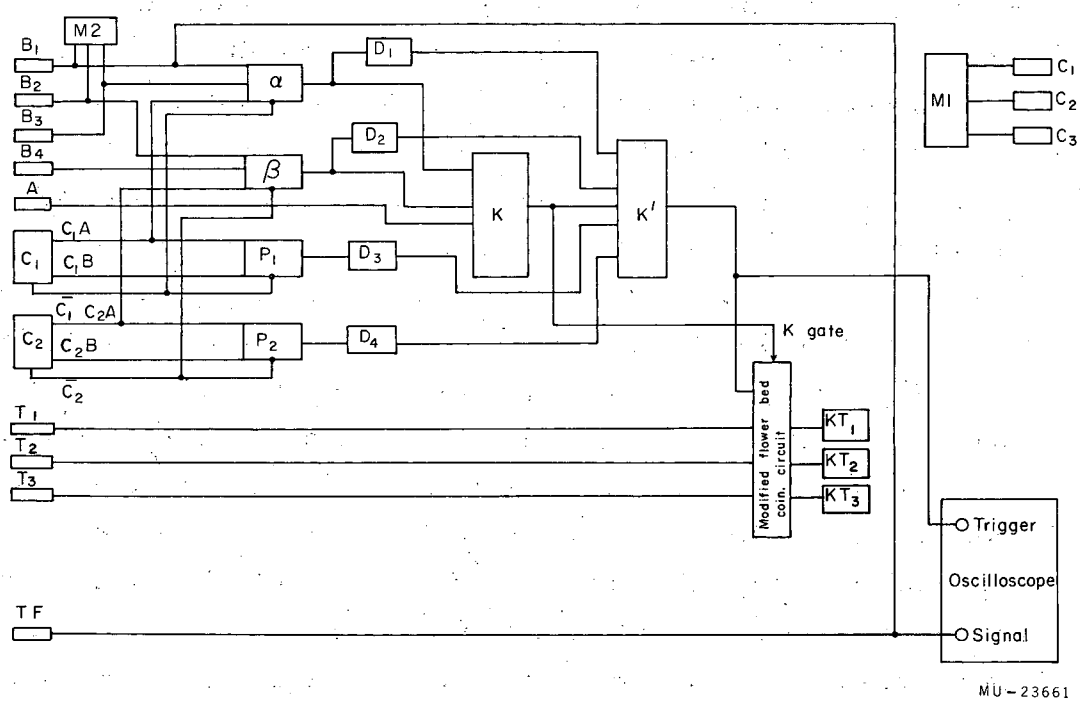

Fig. 5. A simplified schematic drawing showing major electronic components: α, β, P_1, P_2, and K are fast coincidence-anti-coincidence circuits; D_1, D_2, D_3, D_4 are delay boxes. K' is a Garwin coincidence circuit. The modified flowerbed circuit is a multichannel double-coincidence circuit.

The output of the fast coincidence circuits was monitored with Hewlett-Packard prescalers, followed by conventional Lawrence Radiation Laboratory 1-megacycle scalers. The outputs of the slow coincidence circuit and the double-coincidence circuit were directly monitored with 1-Mc scalers.

Two independent monitors were used during the experiment to monitor the beam particles. One monitor, called M1 in Fig. 5, comprising a telescope of three scintillation counters, 3×2×1/2 in. each, was placed in the shielding wall of the Bevatron. This counter-telescope looked directly at the internal Bevatron target. The coincidence rate between the three counters in the telescope gave a good measure of the number of protons striking the internal Bevatron target. The second monitor, M2, was a coincidence counter between the beam counters B_1, B_2, and B_3, and measured the actual beam particles coming down the secondary beam channel.

V. EXPERIMENTAL PROCEDURE

A. General Description

The total cross sections in hydrogen and deuterium were measured by making transmission measurements on the full and empty target. The hydrogen cross sections were measured first. At each momentum, the secondary particle beam was optimized by tuning the magnets in the system and by studying the beam profile at the location of the transmission counters. The Cerenkov counters were then tuned by varying the radiator position and studying the K^- plateau (see Fig. 6). The transmission ratios were measured for the full and empty hydrogen target in alternate runs. In each run, a minimum of 10^4 K^- mesons was counted. The data were recorded after every 5000 K^- counts, and regular checks were made to ascertain that the electronic components were functioning properly. Time-of-flight pictures were taken for both K^- mesons and π^- mesons. The K^- momentum was measured at least twice (once with normal field and then with reversed field in the analyzer magnet) during one setting of the operating momentum with the target flask empty. The origin and rates of accidental counts were fully studied by using various counter combinations and different beam levels.

After the cross sections for hydrogen were obtained for nine different momentum settings, the target flask was emptied of liquid hydrogen and refilled with liquid deuterium. The cross sections for deuterium were then measured for five representative momenta, in the same way as for hydrogen.

B. Identification of K^- Mesons

Figure 7 shows a delay curve obtained when the delays of scintillators B_3 and B_4 were varied with respect to all other counters in the system. K^- mesons are counted with a time resolution curve indicated by the central peak. This rate corresponds to about 2×10^{-3} of the π^- meson rate, and the full width at half-maximum of the timing curve is 10 mμsec. If the timing is off by a large amount, say 50 mμsec, then the K mesons selected by the Cerenkov counters are never

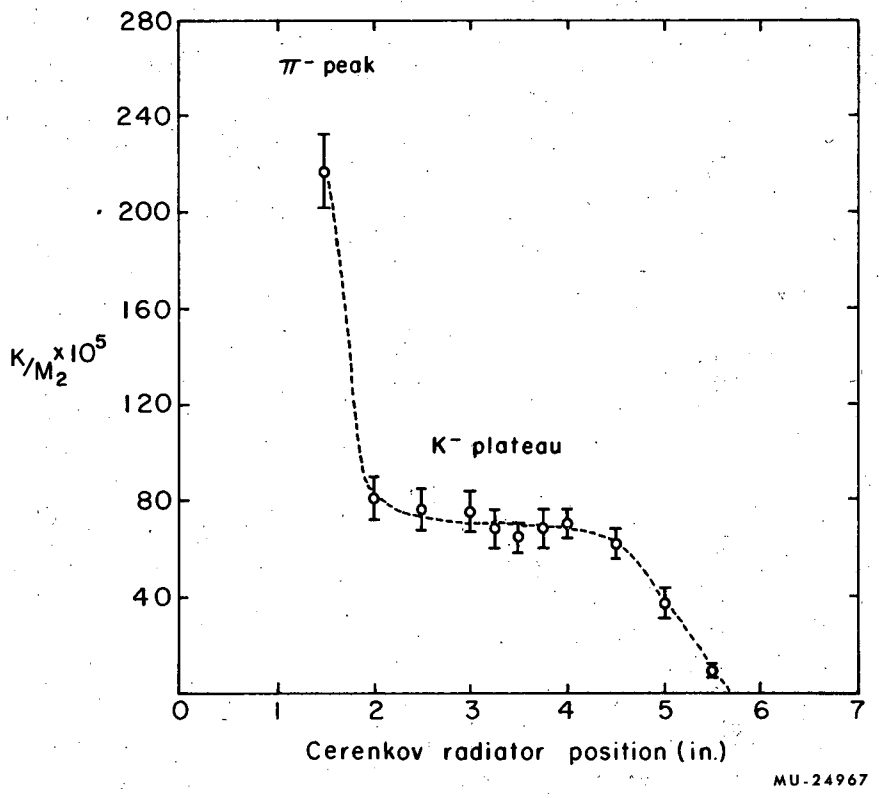

Fig. 6. Cerenkov radiator position-plateauing curve. The K mesons were counted by fixing the radiator position at the center of the approx 3-in. -wide K meson plateau.

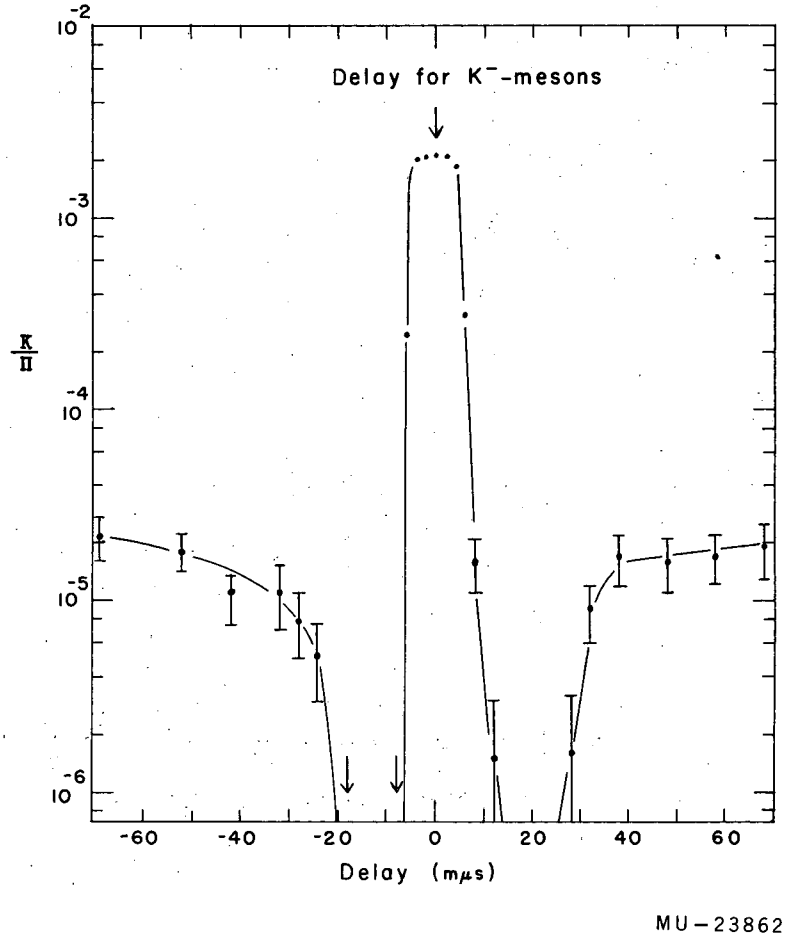

Fig. 7. Delay curve obtained by delaying B_3 and B_4 in the main K-selecting coincidence circuits. This illustrates the effectiveness of the anticoincidence signals from the Cerenkov counter.

counted by the scintillators. There is, however, a steady background at about 1% of the K rate, which is due to accidental coincidence of light mesons present in the beam. However, when the delay is only about ± 10 to ± 20 mμsec, the anticoincidence pulse produced by the off-time particle in the Cerenkov counters results in a reduction of the accidental rate by more than an order of magnitude. Thus, very fast time resolution is not required for the transmission-counter coincidence circuit, as the background accidental rate is roughly three orders of magnitude less than the K rate for times of ± 20 mμsec about the time of arrival of the K mesons.

C. Time-of-Flight Measurement

To confirm the method of identification of K mesons described in Section V-B, and to study the purity of the beam, a check was made on the time of flight of these particles. This was done by comparing the time of flight of those particles identified as K mesons with the π- and μ-meson time of flight. The pulse from the first scintillation counter in the beam B_1, and a pulse from a time-of-flight counter TF placed 42 ft downstream from B_1, were displayed on a Tektronix 517 oscilloscope equipped with a DuMont Oscillograph Record Camera. A simplified diagram of this setup is included in Fig. 5. During one series of runs the oscilloscope was triggered by the "K" signal, using the Cerenkov counters. During another series, the Cerenkov counters were turned off and the trigger was a π signal generated by B_1, B_2, B_3, B_4, and A. Thus the difference in time of flight between π^- mesons and the presumed K^- mesons was determined at several representative momenta. The results not only indicated that the K^- mesons were correctly identified, but also gave a good estimate of the purity of the beam. To obtain an idea of the efficiency of the individual Cerenkov counters, the triggering K signals in several runs were generated by separately switching on C_1 and C_2 in coincidence with the beam counters, and also by switching on C_1 and C_2 together. A few typical time-of-flight histograms so obtained are shown in Figs. 8(A-D). When only C_1 was used,

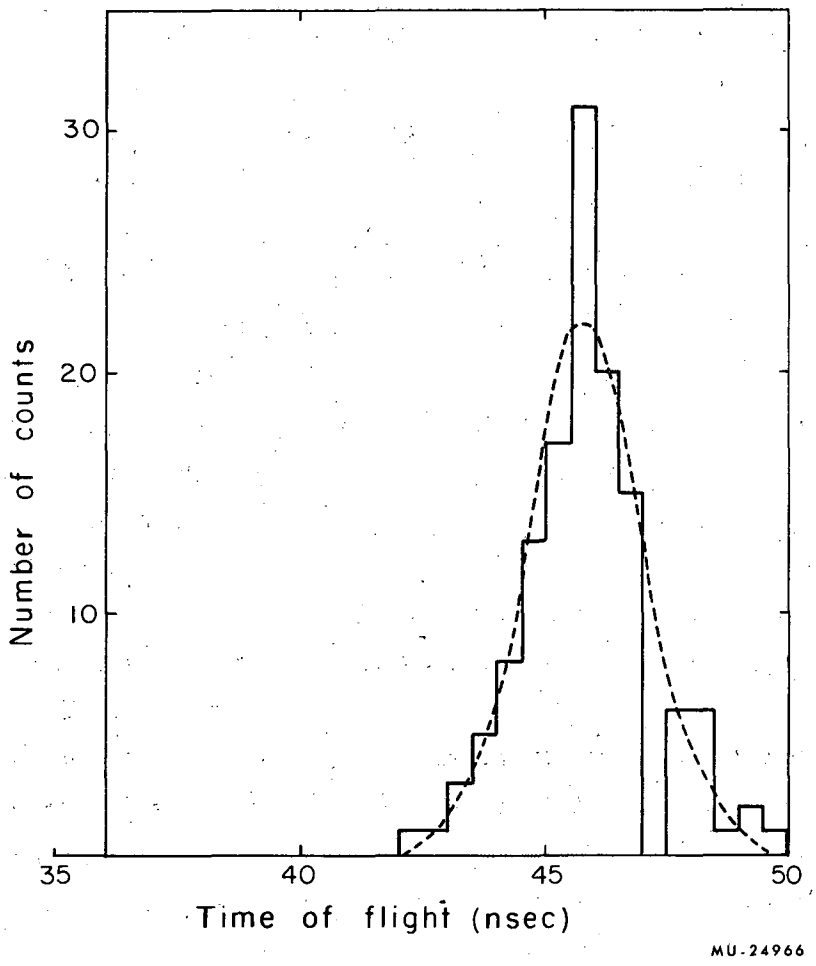

Fig. 8(A). Time-of-flight histogram of K^- mesons at 900 Mev/c nominal momenta, obtained by triggering the oscilloscope with the K signal.

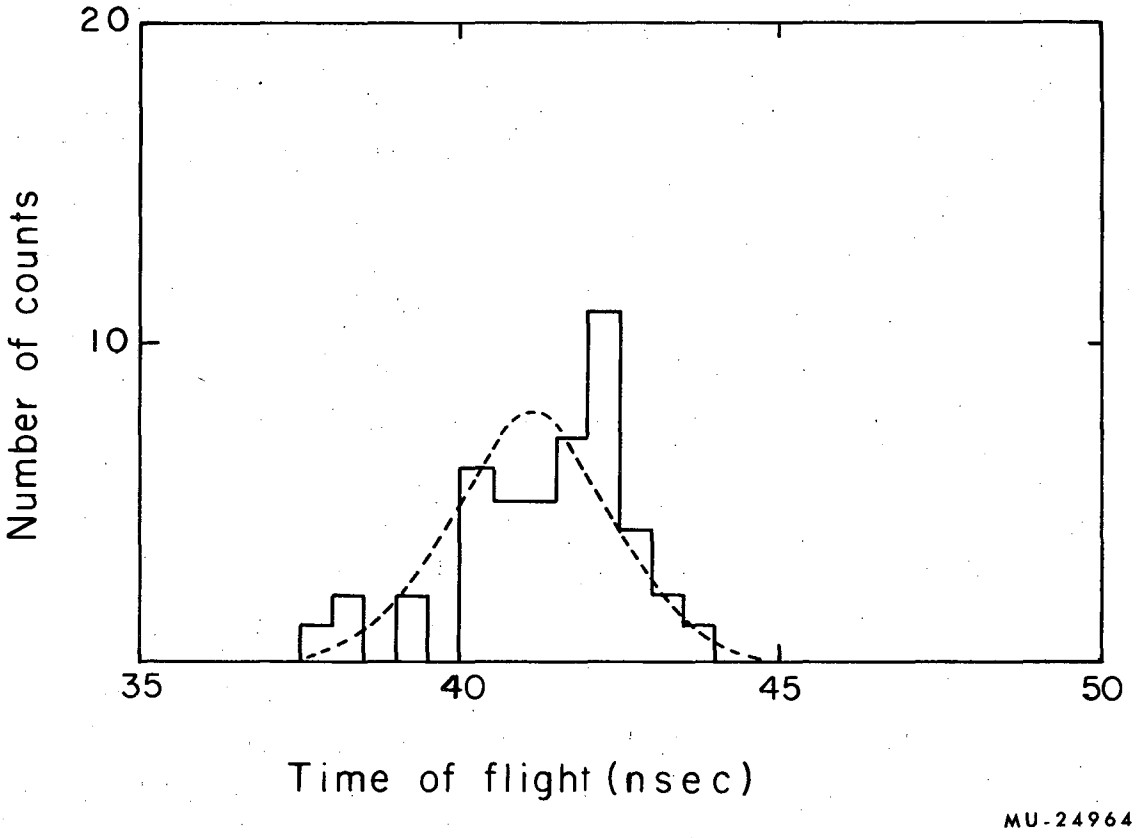

Fig. 8(B). Time-of-flight histogram of π^- mesons at 900 Mev/c nominal momenta, obtained by triggering the oscilloscope with the coincidence of beam counters B_1, B_2, B_3, and B_4.

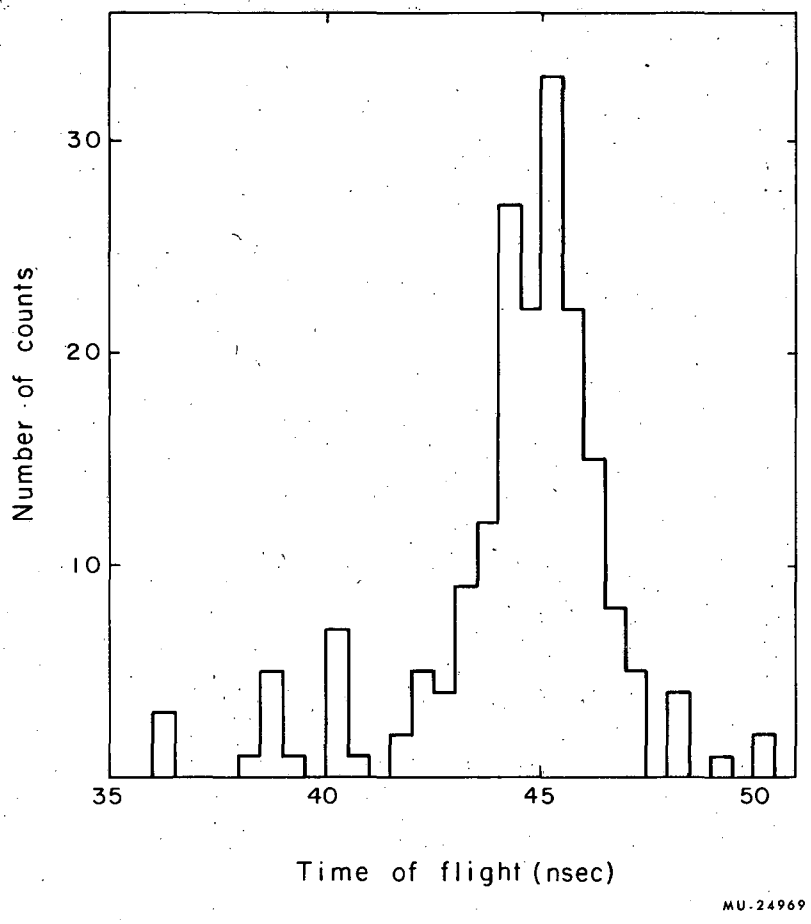

Fig. 8(C). Time-of-flight histogram of K^- mesons at 900 Mev/c, using Cerenkov counter C1 to produce the trigger.

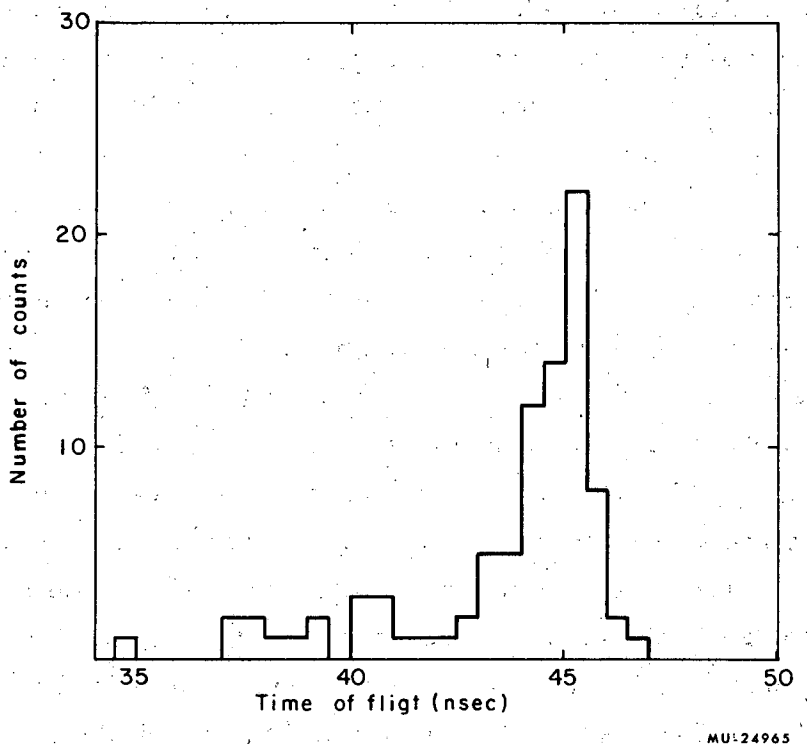

Fig. 8(D). Time-of-flight histogram of K^- mesons at 900 Mev/c, using Cerenkov counter C2 to produce the trigger.

the assumed "K" signals had about 12% π-meson and μ-meson contamination. With C_2 alone the contamination was about 20%. For normal operation, with both C_1 and C_2 switched in, the contamination was about (0.5±0.5)%.

D. Measurement of Momentum

A precise and independent measurement of the beam momentum at the location of the hydrogen target was made by using a 29×36-in. Bevatron analyzer magnet (see Fig. 9). Two vertical strip scintillation counters, P_1 and P_2, were used to define the direction of entrance of the beam particles into the analyzer magnet. Counter P_1 was placed upstream from the hydrogen target and P_2 was placed 119 in. from P_1 and 52 in. from the center of the pole pieces of the analyzer magnet. Downstream from the magnet, and 121 in. from the center of the pole tips, two similar strip scintillation counters, P_3 and P_3', were placed at angles of 25.7 deg with respect to the axis of the beam. The four strip scintillation counters were each 6×1/2×1/8 in. The central momentum, and the spread in momentum of the beam, were determined by studying the threefold coincidence rate between P_1, P_2, and P_3 as a function of the magnet current. To prevent scattered particles from being counted, the triple coincidence of P_1, P_2, and P_3 was put in coincidence with the beam monitor signal (M_2) generated by beam counters B_1, B_2, and B_3. A typical curve so obtained is shown in Fig. 10. To remove possible systematic asymmetries due, for example, to the Bevatron fringe field or hysteresis effects, the measurements were repeated after reversing the field of the magnet and using counter P_3', the mirror image counter of P_3 with respect to the beam line.

The analyzer magnet was calibrated twice, using the floating-wire technique; once before the experimental setup, and again during the experiment with the magnet in place. Calibration values obtained in the two instances agreed within 0.5%. From the calibration curves the resolution of the momentum-analyzing counter system was calculated

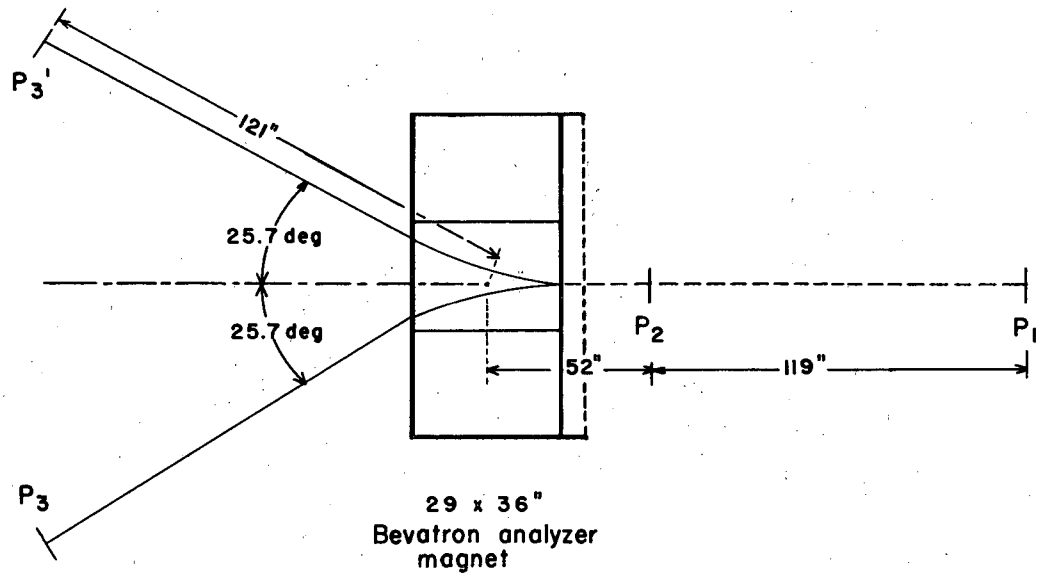

Fig. 9. Arrangement of analyzer magnet and counters to measure the beam momentum. P_1, P_2, P_3, and P_3' are vertical strip scintillation counters each 6 in. × 1/2 in. × 1/8 in. Coincidences P_1, P_2, and P_3 are measured for one sign of the field in the magnet, and coincidences P_1, P_2, and P_3' for the reversed field.

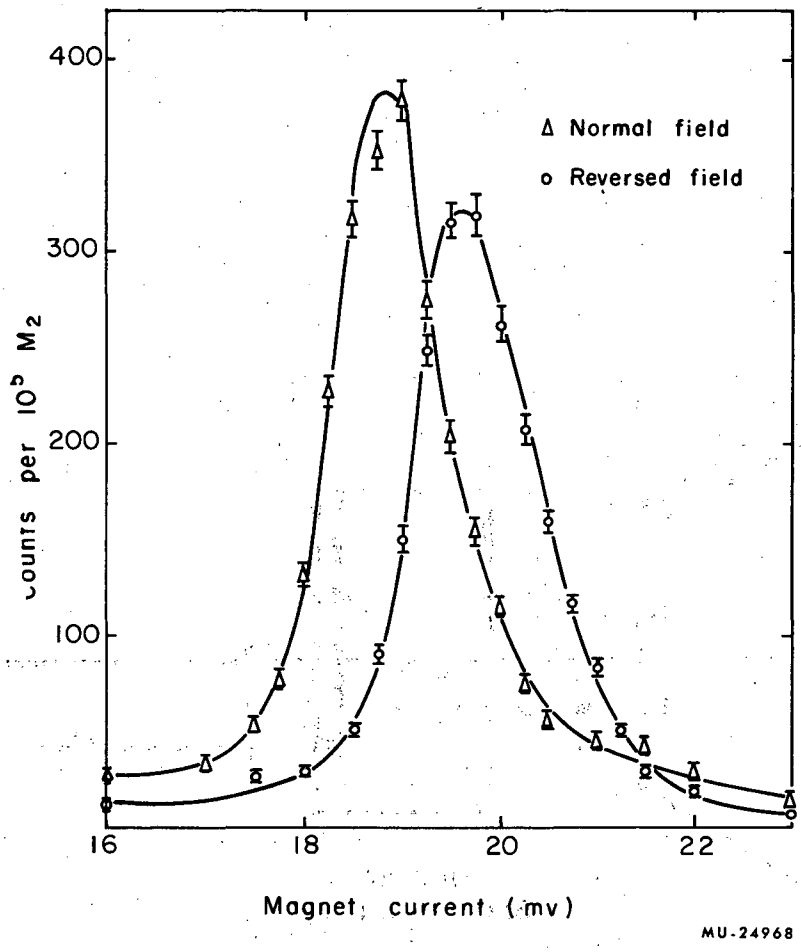

Fig. 10. Typical curves obtained during momentum measurement of the beam particles. One curve is for one sign of the magnetic field, the other is for the reversed field. An average of the two gives the actual momentum of the beam particles passing through the analyzer magnet.

by folding together the resolutions due to (a) the 1/2-in. physical width of the three counters, (b) multiple scattering in the empty hydrogen target assembly, (c) multiple scattering in the three transmission counters, and (d) multiple scattering in the strip counter P_2. The momentum resolution for the worst case, that is, for the lowest momentum measured, was $\pm 3\%$ (half width at half-maximum).

The measured momenta were corrected for (a) the momentum lost in the three transmission counters and the P_2 counter, (b) momentum loss in the 0.032-in. aluminum exit dome and the 0.010-in. Mylar target flask, and (c) momentum loss in 12 in. of liquid hydrogen or deuterium. A correction was also made for the difference in energy loss between π mesons and K mesons, since the measured momenta were primarily those of the beam π mesons. Final values of the momenta are presented in Table I with the measured uncertainties.

Several times during the experiment the momenta were measured with both target full and target empty. Values of momenta so obtained indicated K^- momentum loss of about 20 Mev/c and 25 Mev/c in hydrogen and deuterium respectively, which is in good agreement with calculated values.

Table I. K^- Momentum at the Center of Target.

	Nominal momentum (Mev/c)	Measured momenta (target empty) (Mev/c)	Momentum at center of target[a] (Mev/c)	Number of measurements
Hydrogen				
	700	647	630 ± 2.10%	1
	800	762	752 ± 1.84%	1
	900	848	840 ± 1.45%	3
	950	896	894 ± 1.48%	3
	1000	935	931 ± 3.85%	1
	1050	990	987 ± 2.13%	2
	1100	1030	1030 ± 2.17%	2
	1150	1070	1067 ± 2.05%	2
	1200	1103	1101 ± 1.84%	2
Deuterium				
	700	646	627 ± 1.53%	2
	800	763	750 ± 2.14%	1
	900	815	808 ± 2.46%	1
	1050	988	984 ± 2.44%	1
	1150	1067	1067 ± 1.52%	3

[a]Measured momenta were corrected for the appropriate momentum loss in the target and transmission counters to obtain the K^- momenta at the center of the target.

VI. THE YIELD OF K^- MESONS

During typical operation, the number of negatively charged particles passing down the beam channel was between 2×10^4 and 6×10^4 per Bevatron pulse of about 1.5×10^{11} protons. The number of K^- mesons counted per Bevatron pulse ranged from 5 to 30 in the momentum range involved. As can be seen from the beam layout (Fig. 2), there was a large number of scattering objects in the beam. The major contribution in scattering came from the 2-in.-thick Cerenkov radiators. The attenuation of K mesons due to scattering as well as decay in flight was larger at the lower momenta than at the higher. Figure 11 shows the K/π ratios actually recorded during the experiment (see also Table II). The counting rate of K^- mesons depended on the radiator material used in the Cerenkov counters. For momenta below 900 Mev/c the radiator was lucite, and for 900 Mev/c and above it was liquid Fluorochemical (FC-75). The relative difference in the efficiencies is obvious from Fig. 11. No measurements were made to calculate the absolute efficiencies of the Cerenkov counters with different radiators.

The number of K^- mesons counted was corrected for decay in flight and multiple Coulomb scattering. The results are presented in Table II. Since the internal proton beam was not accurately known, the absolute magnitudes of the results given in Table II are correct only within a factor of 2.

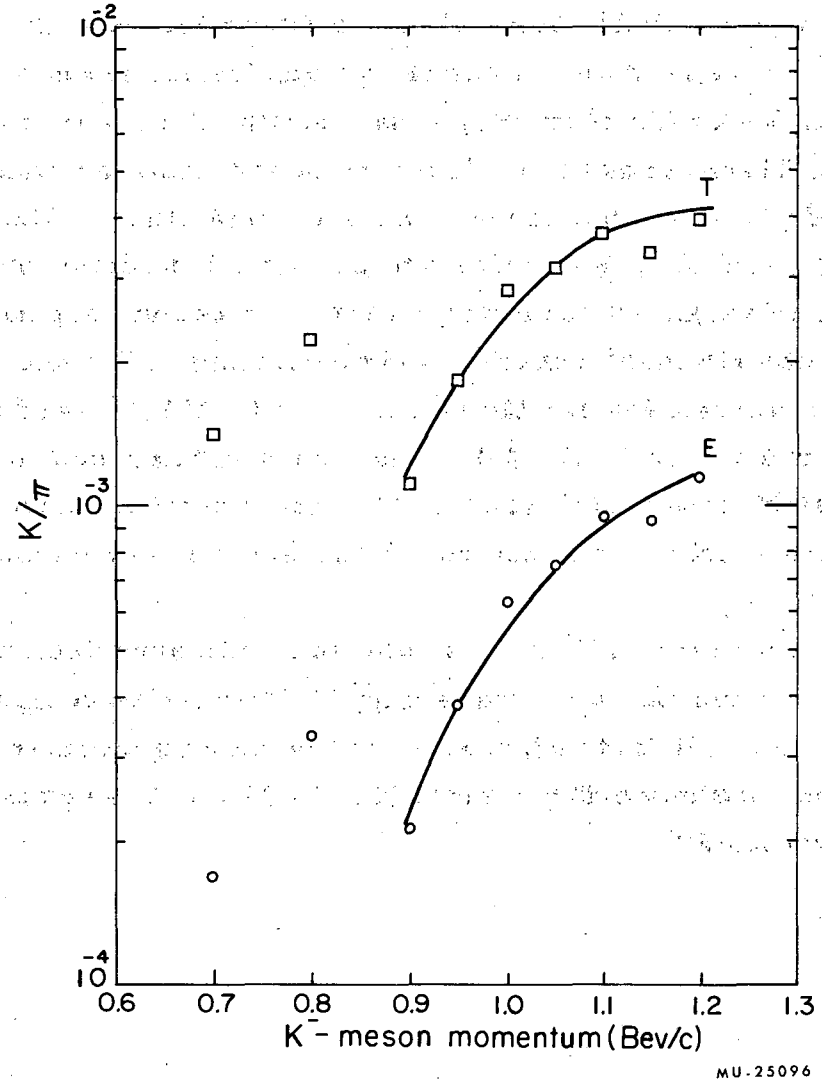

Fig. 11. Production of K^- mesons at different momenta. Curve E gives actually counted K/π ratios during the run. Curve T is the K/π ratio at the Bevatron internal target, obtained by correcting the actual counts for decay in flight.

Table II. Summary of the main characteristics of the secondary beam at different momenta: column 1 gives the momentum of the beam at production.

Momentum p (Mev/c)	Momentum spread $(\Delta p)/p$ (%)	Emission angle (rad)	K/π at target[a]	K/p at target[b] (correct within a factor of 2) (per msr)	Mean proton energy, $\bar{E}_p$ (Bev)
700	4.2	0.105	1.43×10^{-3}	7.1×10^{-9}	4.8
800	3.6	0.105	2.13×10^{-3}	9.4×10^{-9}	4.8
900	2.9	0.105	1.12×10^{-3}	4.7×10^{-9}	4.8
950	2.9	0.105	1.85×10^{-3}	6.8×10^{-9}	4.8
1000	3.9	0.105	2.82×10^{-3}	9.7×10^{-9}	4.8
1050	4.2	0.105	3.14×10^{-3}	9.3×10^{-9}	4.8
1100	4.4	0.105	3.70×10^{-3}	9.1×10^{-9}	4.8
1150	4.1	0.105	3.38×10^{-3}	9.4×10^{-9}	4.8
1200	3.6	0.105	3.97×10^{-3}	8.2×10^{-9}	4.8

[a] Both K's and π's were corrected for decay in flight to obtain ratio at target.

[b] The counted K's were corrected for decay in flight and multiple Coulomb scattering to obtain number of K^- mesons produced at target.

VII. CALCULATION OF THE TOTAL CROSS SECTION

The total cross section, σ, may be expressed:

$$\sigma = \frac{1}{nL} \ell n \frac{t_E}{t_F} ,$$

where

n = number of target nuclei per cm^3,

L = length of target,

t_E = target-empty transmission factor,

and

t_F = target-full transmission factor.

The statistical error in σ arising from the uncertainty in the transmission factor is given by

$$\Delta\sigma = \frac{1}{nL} \left[\left(\frac{\Delta t_E}{t_E}\right)^2 + \left(\frac{\Delta t_F}{t_F}\right)^2 \right]^{1/2} .$$

Under the pressure and temperature conditions at which the target was operated, the mass of the gas in the "empty" target was not entirely negligible compared with the mass of the liquid in the "full" target. Thus the atomic concentration n refers to the difference in atomic concentrations between liquid and gas in the target. As described in Section IV, three separate transmission counters were used after the target. The first two were circular in shape and 7 and 9 in. in diam respectively; the third was a 13-in.-square counter. Thus each counter subtended a different solid angle at the target. The cross sections obtained from each counter depended on the solid angle subtended by the counter (see Fig. 12). Before any corrections, were applied, the measured cross sections were extrapolated to zero solid angle, and the total cross sections so obtained are shown in Table III, just for comparison with the final values.

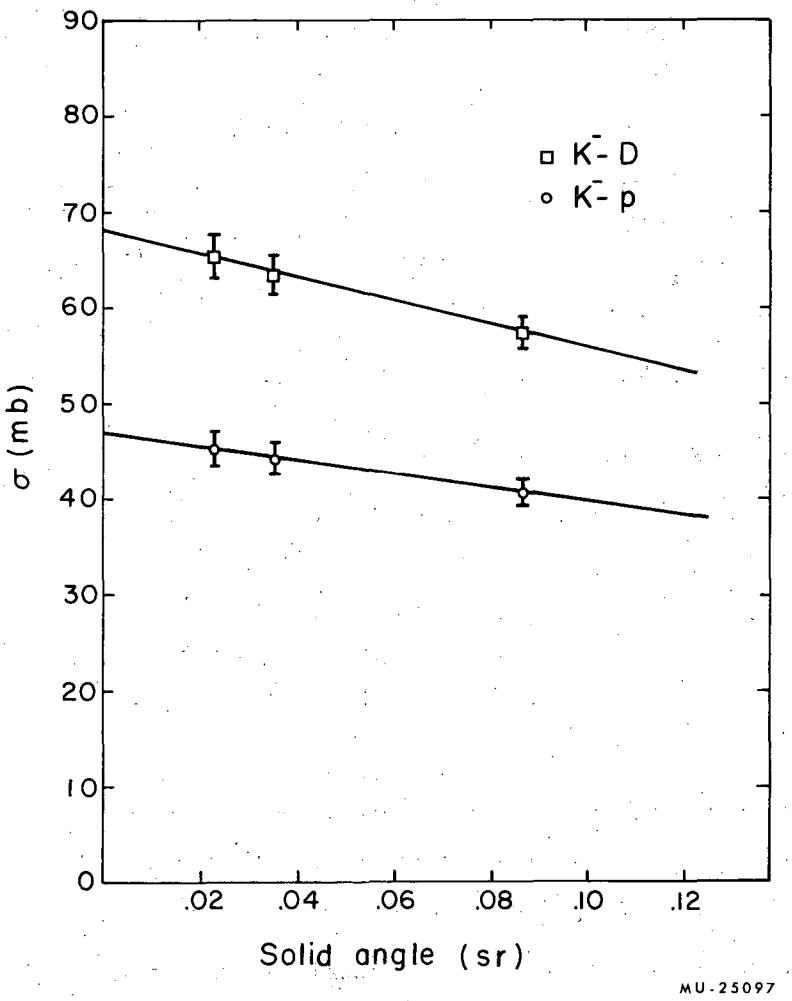

Fig. 12. Solid angle subtended by the transmission counters vs measured uncorrected total cross sections (only accidental corrections included) at 900 Mev/c nominal momenta. Note the linear dependence of both K^--p and K^--d total cross sections.

Table III. Total cross sections obtained by extrapolating to zero solid angle (Each transmission counter subtending a different solid angle).

Nominal momenta (Mev/c)	σ_A [a] (mb)	σ_B [b] (mb)
K^--p total cross sections		
700	41.3 ± 4.48	34.8 ± 3.86
800	40.2 ± 3.34	38.0 ± 2.97
900	42.6 ± 3.18	40.5 ± 2.77
950	45.7 ± 4.28	43.5 ± 3.73
1000	47.0 ± 3.09	44.7 ± 2.68
1050	48.3 ± 3.58	46.8 ± 3.10
1100	51.0 ± 3.20	49.7 ± 2.79
1150	53.5 ± 3.41	51.3 ± 3.05
1200	46.8 ± 2.89	45.6 ± 2.60
K^--D total cross sections		
700	65.0 ± 5.94	58.9 ± 5.27
800	69.7 ± 4.47	66.6 ± 4.10
900	68.1 ± 3.93	65.3 ± 3.67
1050	83.8 ± 3.62	83.7 ± 3.62
1150	82.5 ± 2.24	81.9 ± 2.76

[a] σ_A is the total cross section obtained by extrapolating accidental corrected cross sections to zero solid angle.

[b] σ_B is the total cross section obtained by extrapolating to zero solid angle the resulting cross sections after all corrections have been applied.

The subtraction of full- and empty-target data does not exactly cancel all background effects, and the corrections listed below were applied to the measured numbers before we arrived at the results presented in Table IV. The magnitudes of the corrections are listed in Tables V through VIII.

A. Accidental Counts and Rate Sensitivity

The delay curve shown in Fig. 5 illustrates the effect of the Cerenkov counter anticoincidence counting in suppressing off-time accidental counts that could arrive within the resolution time of the transmission counters. Another source of accidental background arose from particles passing outside the Cerenkov radiators and so not having the protection of the anticoincidence. The origin of accidental counts was fully studied by use of a pulser and various combinations of counters. The accidental rates and rate sensitivity were measured at different beam levels. The cross sections at different beam levels showed no significant correlation to the counting rate (see Fig. 13).

The true transmission factor t is given by the expression

$$t = \frac{T - \epsilon T_{acc}}{K - \epsilon T_{acc}},$$

where

T = coincidence counts between a transmission counter signal and the K^- signal,

T_{acc} = accidental coincidence counts between the transmission counter and the K^- signal,

K = number of K^- meson counts,

and

ϵ = a weighting factor obtained from the study of the origin of accidental counts, using a pulser.

The measured weighting factor ϵ was different for different radiators in the Cerenkov counters and also different for the three separate transmission counters. Its value depended additionally on whether the beam anticoincidence counter A was present or not. The values of ϵ obtained from measurement are presented in Table IX.

Table IV. Calculated total cross sections for the three counters at different momenta.

Nominal momenta (Mev/c)	σ_1 (mb)		σ_2 (mb)		σ_3 (mb)	
	uncorrected	corrected	uncorrected	corrected	uncorrected	corrected
K^--p total cross sections						
700	---	---	38.92	34.99±2.82	35.50	35.35±2.64
800	---	---	38.32	37.09±2.22	35.56	35.52±1.97
900	39.04	39.56± 1.86	35.79	36.21±1.52	30.20	33.87±1.38
950	42.46	42.48± 2.52	41.48	42.16±2.09	35.73	39.53±1.79
1000	43.89	44.00± 1.65	42.95	43.62±1.59	36.97	41.72±1.38
1050	45.09	45.12± 1.89	44.58	44.89±1.81	39.00	41.15±1.66
1100	48.03	48.56± 1.72	46.48	48.08±1.65	40.48	45.70±1.46
1150	48.81	50.48± 1.87	46.71	48.66±1.79	39.18	46.28±1.62
1200	44.06	44.44± 1.60	43.17	44.39±1.51	37.71	41.88±1.38
K^--D total cross sections						
700	62.33	57.65± 3.10	59.83	57.43±3.07	54.59	54.60±2.85
800	66.90	65.83± 2.48	64.80	64.57±2.39	58.89	62.82±2.23
900	63.55	63.51± 2.32	60.90	62.99±2.22	52.70	59.14±1.77
1050	78.05	81.57± 2.19	74.88	80.35±2.10	63.81	75.62±1.98
1150	77.79	81.85± 1.59	74.79	80.35±1.56	65.99	80.24±1.63

Table V. Accidental corrections applied for the three counters at different momenta.

Nominal momenta (Mev/c)	$\Delta\sigma_1$ (mb)	$\Delta\sigma_2$ (mb)	$\Delta\sigma_3$ (mb)
Hydrogen			
700	---	0.97	2.20
800	---	0.44	1.04
900	2.09	1.53	3.33
950	1.76	1.73	3.86
1000	1.40	1.25	3.64
1050	0.59	0.60	0.85
1100	0.96	1.05	2.65
1150	2.09	1.75	4.26
1200	0.51	0.76	1.35
Deuterium			
700	0.84	0.81	1.86
800	0.82	0.90	2.37
900	1.80	2.59	4.72
1050	2.17	2.48	5.23
1150	2.40	2.24	5.63

Table VI. - Forward scattering corrections applied for the three counters at different momenta.

Nominal momenta (Mev/c)	$\Delta\sigma_1$ (mb)	$\Delta\sigma_2$ (mb)	$\Delta\sigma_3$ (mb)
Hydrogen			
700	-	0.40 ± .04	0.88 ± .09
800	-	0.54 ± .05	1.17 ± .12
900	0.49 ± .05	0.62 ± .06	1.23 ± .12
950	0.64 ± .06	0.93 ± .09	1.93 ± .19
1000	0.73 ± .07	1.06 ± .11	2.21 ± .22
1050	0.83 ± .08	1.25 ± .13	2.39 ± .24
1100	1.04 ± .10	1.51 ± .15	3.05 ± .31
1150	1.21 ± .12	1.68 ± .17	3.33 ± .33
1200	0.99 ± .10	1.47 ± .15	2.86 ± .29
Deuterium			
700	0.64 ± .06	0.91 ± .09	1.93 ± .19
800	1.06 ± .11	1.53 ± .15	3.26 ± .33
900	1.14 ± .11	1.65 ± .17	3.33 ± .33
1050	2.56 ± .26	3.64 ± .36	7.13 ± .71
1150	3.01 ± .30	4.26 ± .43	9.04 ± .90

Table VII. Decay-in-flight corrections applied for the three counters at different momenta.

Nominal momenta (Mev/c)	$\Delta\sigma_1$(mb)		$\Delta\sigma_2$(mb)		$\Delta\sigma_3$(mb)	
	1st order	2nd order	1st order	2nd order	1st order	2nd order
Hydrogen						
700	-	-	3.92	4.12	4.07	3.10
800	-	-	3.38	1.55	2.49	2.25
900	1.72	1.06	1.78	1.40	1.86	0.89
950	1.50	1.49	1.59	1.75	1.62	1.94
1000	1.34	1.38	1.39	1.34	1.45	1.10
1050	1.16	0.95	1.21	1.29	1.26	1.09
1100	1.07	1.13	1.11	0.77	1.15	0.48
1150	0.99	1.34	1.03	1.23	1.08	0.49
1200	0.93	0.86	0.96	0.75	1.00	0.04
Deuterium						
700	3.97	4.10	4.11	3.61	4.28	3.78
800	2.43	1.62	2.52	2.06	2.63	1.70
900	1.99	2.08	2.06	1.50	2.15	1.61
1050	1.25	0.74	1.29	0.51	1.35	0.53
1150	1.04	1.04	1.08	0.88	1.12	0.42

Table VIII. Corrections applied due to multiple coulomb scattering and beam divergence for the three counters at different momenta.

Nominal momenta (Mev/c)	$\Delta\sigma_1$ (mb)	$\Delta\sigma_2$ (mb)	$\Delta\sigma_3$ (mb)
Hydrogen			
700	-	1.18	0.12
800	-	0.66	0
900	1.00	0.33	0
950	0.88	0.22	0.05
1000	0.64	0.30	0
1050	0.44	0.25	0
1100	0.34	0.19	0
1150	0.29	0.25	0
1200	0.26	0.26	0
Deuterium			
700	2.06	0.51	0
800	1.33	0.60	0
900	0.90	0.65	0
1050	0.47	0.14	0.02
1150	0.31	0.06	0

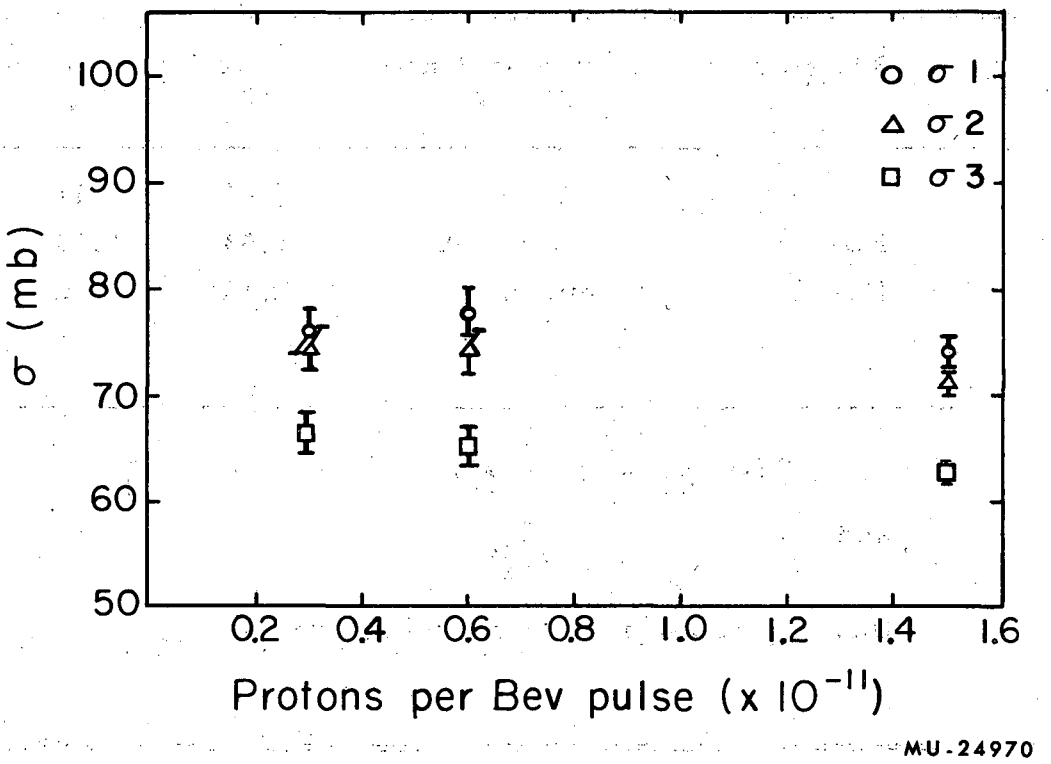

Fig. 13. Measured K^--D cross section vs proton beam intensity at 1150 Mev/c nominal momenta for the three transmission counters. Within statistical errors the cross sections do not depend on beam level.

Table IX. The weighting factor ϵ for accidental corrections[a] (see Section VII-A).

Radiator	Anticoincidence counter	Transmission counters T_1	T_2	T_3
Lucite	without A	0.24	0.31	0.46
FC-75	without A	0.53	0.54	0.68
FC-75	with A	0.10	0.12	0.25

[a] Let $\gamma_E = \epsilon \left(\frac{T_{acc}}{K}\right)_E$,

and

$$\gamma_F = \epsilon \left(\frac{T_{acc}}{K}\right)_F;$$

then ϵ is as given in the table above.

If we now define the quantities

$$\gamma_E = \epsilon \left(\frac{T_{acc}}{K}\right)_E$$

and

$$\gamma_F = \epsilon \left(\frac{T_{acc}}{K}\right)_F$$

for the empty and full target respectively, the true target-empty and target-full transmission factors become

$$t_E = \frac{T_E - \gamma_E}{1 - \gamma_E}$$

and

$$t_F = \frac{T_F - \gamma_F}{1 - \gamma_F},$$

where T_E and T_F are the transmission factors $(T/K)_E$ and $(T/K)_F$ actually recorded during the experiment. The total cross section is therefore

$$\sigma_{corrected} = \frac{1}{nL} \ell n \frac{t_E}{t_F} = \frac{1}{nL} \ell n \frac{T_E}{T_F} \frac{1-\gamma_E/T_E}{1-\gamma_F/T_F} \frac{1-\gamma_F}{1-\gamma_E},$$

or

$$\sigma_{corrected} = \sigma_{uncorrected} + \frac{1}{nL} \ell n \frac{1-\gamma_E/T_E}{1-\gamma_F/T_F} \frac{1-\gamma_F}{1-\gamma_E}.$$

The correction due to accidental coincidences is then given by

$$\Delta\sigma_{acc} = \sigma_{corrected} - \sigma_{uncorrected} = \frac{1}{nL} \ell n \frac{1-\gamma_E/T_E}{1-\gamma_F/T_F} \frac{1-\gamma_F}{1-\gamma_E}.$$

The values of this correction are presented in Table V. The correction ranged from 0.5 mb to 5 mb; they were smallest for counter T_1 and largest for T_3.

B. Forward Scattering

K^- mesons interacting in the target can still be counted by the transmission counters if they are scattered through a small angle ($\leq$ 5 deg). From the optical theorem,[12] the imaginary part of the forward-scattering amplitude, Im f(0 deg) is given by

$$\text{Im } f\ (0 \text{ deg}) = \frac{k\sigma}{4\pi} ,$$

where σ is the total cross section and k the wave number. Thus the differential-scattering cross section per unit solid angle is

$$\frac{d\sigma}{d\Omega}\ (0 \text{ deg}) \geq \left[\frac{k\sigma}{4\pi}\right]^2 .$$

In the absence of any data on the real part of the forward-scattering amplitude the differential-scattering cross section per unit solid angle in the forward direction was assumed to be equal to the lower limit $(k\sigma/4\pi)^2$ given by the optical theorem. This correction was multiplied by a factor of approximately 1.1 to take account of double scattering in the liquid hydrogen or deuterium and in the aluminum jacket of the target. The corrections are presented in Table VI. In the worst case, the correction for hydrogen was less than 1.2 mb for the smallest counter and less than 3.5 mb for the largest; for deuterium these numbers were 3 mb and 9 mb respectively.

The real part of the forward-scattering amplitude as a function of momentum is not known at present. Its magnitude can be estimated from the available data. Cook et al. measured the K^--p elastic scattering at K^- laboratory momentum 1.95 Bev/c, and obtained a value for the real part of 0.56± 0.10 fermi.[5] The low-energy scattering data of Bastien et al. also give values of about the same order of magnitude.[6] If we assume the real part to be 0.56 fermi, the forward-scattering corrections should be increased by 7.5%. To account for this, we assume the uncertainty in the forward-scattering corrections to be 10% of the corrections applied.

C. Decays in Flight

A considerable fraction of K^- mesons undergoes decay in flight between the last Cerenkov counter and the transmission counter. A larger fraction decays at the lower momenta than at the higher. In the lowest order, this effect is removed by the subtraction between target-full and target-empty data, but three higher-order corrections need to be applied. The largest of these arises from the energy degradation in the full target, which enhances slightly the rate of decay between the target and transmission counters. The other two corrections involve the small fraction of decay products striking the counters and simulating a K^- meson count. The decay products originating ahead of or within the target suffer some attenuation in the full target, whereas those originating later have a slightly increased chance of being counted because the K^- mesons have been slowed down in the liquid hydrogen or deuterium in the target. Since all the pertinent parameters are well known, these corrections can be calculated exactly. The detailed derivations are given in Appendix B.

The first-order correction in which we assume that all the decay products are lost is given (see Eq. B-9) by

$$\sigma_{\text{1st order}} = \sigma_{\text{uncorrected}} - \frac{1}{nL}\left(\frac{x}{24.37}\,\frac{\Delta p}{p^2}\right),$$

where x is the distance from the center of the hydrogen target to the transmission counter, p is the K^- momentum at the center of the target, and Δp is the momentum loss by the K^- mesons in passing through the liquid hydrogen or deuterium in the target. If we include the probability of detecting a fraction of the K^- decay products in the transmission counters, the corrected total cross section becomes

$$\sigma = \frac{1}{nL}\,\ell n\left[\frac{A + B}{\dfrac{\exp[-x_2/\lambda] + C}{T_E/T_F}} - D\right],$$

where

$$A = \exp - [x_2 - x_1]/\lambda \quad \exp[-x_1/\lambda']$$

$$B = \frac{1}{\lambda'} \sum_i B_i \int_{x_2 - x_1}^{x_2} \exp[-x/\lambda'] \; P_i' \left\langle \theta'(x) \right\rangle \, dx,$$

$$C = \frac{1}{\lambda} \sum_i B_i \int_0^{x_2} \exp[-x/\lambda] \; P_i \left\langle \theta(x) \right\rangle dx,$$

$$D = \frac{1}{\lambda} \sum_i B_i \int_0^{x_2 - x_1} \exp[-x/\lambda] \; P_i \left\langle \theta(x) \right\rangle dx.$$

Since the derivations are complicated, only the final expressions are presented here (for detail, see Appendix B). The distances x_1 and x_2 are defined as shown in Fig. 18. Quantities λ and λ' are the mean decay lengths for the K^- mesons before and after they pass through the target. The B_i is the K^- branching ratio for the ith decay mode, and $P_i \left\langle \theta(x) \right\rangle$ is the probablity of detecting a charged decay product from the ith decay mode of a K^- meson decaying at position x. The expressions for the probability $P_i \left\langle \theta(x) \right\rangle$ were substituted for the different decay modes following Blaton,[13] and Baldin et al.[14] The integrals were computed on the IBM 704 for all the fifteen different momentum settings used in the experiment.

The decay-in-flight corrections for the measured cross sections are presented in Table VII. The corrections ranged from 0.04 mb at the lowest value of the momentum to 4 mb at the highest. In this case, the correction was largest for the T_1 counter and smallest for the T_3 counter.

D. Multiple Coulomb Scattering and Beam Divergences

When the target is full, multiple Coulomb scattering in the hydrogen or deuterium increases the size of the beam at the location of the transmission counters. To correct for this effect, the spatial distribution of the beam was explored at each momentum setting, by use of a 1/2-in.-sq scintillation counter. One such beam distribution, measured at 700 Mev/c, is shown in Fig. 14.

A general method for applying multiple Coulomb scattering correction to experiments of this type is described by R. M. Sternheimer.[15] Barkas and Rosenfeld give an improved expression for the Coulomb scattering.[16] Their method assumes that Coulomb scattering has a Gaussian distribution in angle, with a root-mean-square space angle θ_{rms} given by

$$\theta_{rms} = \frac{15\ (\text{Mev})}{p\ v\ (\text{Mev})} \sqrt{L/L_{rad}}\ (1 + \epsilon)\ \text{radians},$$

where p and v are the momentum and velocity of the particle respectively, L/L_{rad} is the thickness of the scatterer in units of radiation lengths, and ϵ is a correction factor (tabulated in reference 16). The factor ϵ is a function of the particle velocity, and also the thickness and the nuclear charge Z of the scatterer.

The calculations for multiple Coulomb scattering correction were carried out as follows. If we have a beam distribution $F(r)$ whose intensity depends only on the distance r from the beam axis, the total number of particles passing through a circular counter of radius R is given by

$$N_E = 2\pi \int_0^R F(r)\ r\ dr = \int_0^R H(r)\ dr,$$

where $H(r) = 2\pi\ r\ F(r)$. When the target is full, the liquid hydrogen or deuterium scatters out some of the particles. Assuming that Coulomb scattering has a Gaussian distribution in angle, the number of particles

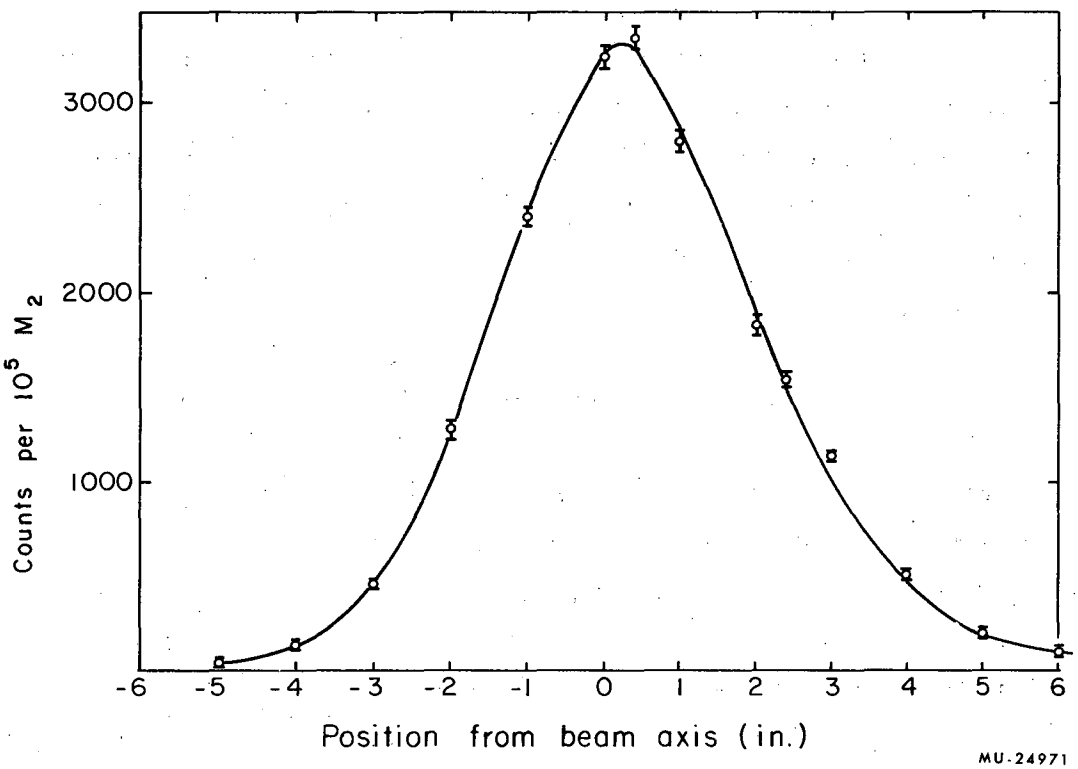

Fig. 14. Horizontal beam profile obtained by using a 1/2-in. -sq scintillation counter. The vertical profile is very similar to the horizontal.

passing through the counter when the target is full can be calculated. The true transmission factors can then be written down in terms of these results, and the cross sections obtained. The derivations are presented in Appendix C. The resulting expression for the multiple Coulomb scattering correction is

$$\Delta\sigma = \sigma_{\text{uncorrected}} - \sigma_{\text{corrected}} = \frac{1}{nL}\frac{r_m^2}{2N_E}\left[\frac{dH(r)}{dr}\right]_R ,$$

where r_m is the projected root-mean-square radius at the location of the transmission counter (obtained from θ_{rms}), and n and L represent the same quantities as defined before.

The measured beam distributions showed that the K^- beam was very nearly symmetric about the beam axis. For example, the widths of the distributions at 700 Mev/c were 3.75 in. and 3.5 in. for the horizontal and vertical distributions respectively (full width at half-maximum). Therefore it was decided to calculate the corrections by using the formulas for a distribution symmetrical about the beam axis, but using both the measured horizontal and vertical distributions. Thus we obtain a total of four different corrections for each momentum setting; two from each of the measured distributions. An average of the four corrections is taken as the magnitude of the final Coulomb scattering correction to be applied. The corrections are shown in Table VIII. Magnitude ranged from 0 to 1 mb for hydrogen, and 0 to 2 mb for deuterium; smallest for transmission counter T_3 and largest for T_1.

E. Light-Particle Contamination

The presence of light mesons in the beam can affect the measured K^- total cross sections. Beam contamination was measured by taking time-of-flight pictures as described in Section V-C, and we found that $0.5 \pm 0.5\%$ π^- mesons were present in the K^- beam. The correction due to π^--meson contamination in the beam is given by the expression

$$\frac{T_F}{T_E} = (1-\delta) \exp [-n\sigma_K L] + \delta \exp[-n\sigma_\pi L],$$

where T_F/T_E is the ratio of target-full and target-empty transmission factors, δ is the fraction of the beam that is π^- mesons, and σ_K and σ_π are the K^- and π^- total cross sections, respectively. It can be seen from the above expression that the correction is zero, if $\sigma_K = \sigma_\pi$. Actual values of the π^- total cross sections were used to calculate the corrections from the above expression. Since δ is small (0.005 ± 0.005), the correction due to π^- contamination in the beam is less than 0.3 mb, and is therefore negligible compared with the other correction terms described in previous sections.

All the above corrections were applied to both the K^--p and K^--d cross sections. The cross sections so obtained for the individual counters are presented in Table IV. As can be seen there, the corrections did not completely remove the dependence of the cross sections on the solid angles subtended by the counters. However, in some cases the dependence either diminished or became uncorrelated. Hence further analysis of the results is required before arriving at the final magnitudes of the total cross sections.

There were only two transmission counters (T_2 and T_3) present when we measured the hydrogen cross section at 700 and 800 Mev/c (nominal momenta). At the higher end of the momentum region involved, the forward scattering correction becomes large for the largest counter; at the lower end the multiple Coulomb scattering correction becomes large for the smallest counter. After studying the differences in measured cross sections $(\sigma_1-\sigma_2)$ and $(\sigma_2-\sigma_3)$ we decided to calculate the final cross sections as follows (where σ_1, σ_2, σ_3 are the total cross section obtained from transmission counters T_1, T_2, T_3 respectively): (a) weighted average of σ_2 and σ_3 for 700 and 800 Mev/c in hydrogen and 700, 800, 900 Mev/c in deuterium, (b) weighted average of σ_1, σ_2, and σ_3 for 900 and 1150 Mev/c in hydrogen, and (c) weighted average

of σ_1 and σ_2 for all other momenta. The final magnitudes of total cross sections are presented in Tables X and XI and plotted together with other available data in Figs. 15 and 16.

Table X. K^--p total cross sections[a]

K^- meson momenta, lab system (Mev/c)	Total cross section (mb)
630	35.18 ± 1.93
752	36.21 ± 1.47
840	36.01 ± 0.90
894	42.28 ± 1.61
931	43.80 ± 1.14
987	44.99 ± 1.31
1030	48.30 ± 1.19
1067	48.27 ± 1.01
1101	44.41 ± 1.10

[a] See text (Section VII) for description of how these total cross sections were calculated.

Table XI. K^--D and K^--n total cross sections[a]

K^--meson momenta, lab system (Mev/c)	K^--D total cross sections (mb)	K^--n total cross sections (mb)
627	55.86 ± 2.09	22.94 ± 3.06
750	63.62 ± 1.63	30.44 ± 2.35
808	63.23 ± 1.60	30.21 ± 2.00
984	80.93 ± 1.52	41.02 ± 2.18
1067	81.08 ± 1.11	37.83 ± 1.65

[a] See text (Section VIII) for description of how these total cross sections were calculated.

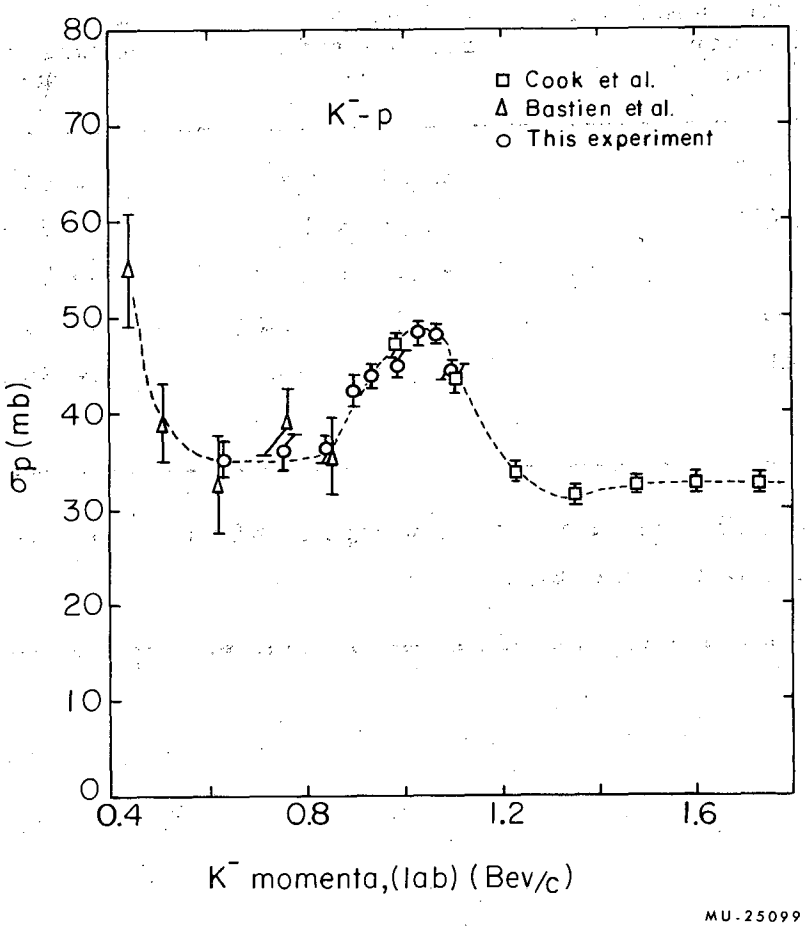

Fig. 15. The K^--p total cross sections plotted together with some of the data from the experiment of Cook et al.,[5] and some preliminary data of Bastien et al.[6] (I would like to thank Professor Robert D. Tripp for communicating the unpublished data from his group). The resonant peak appears about 15 mb above the nonresonant background of approx 35 mb (see also Table X).

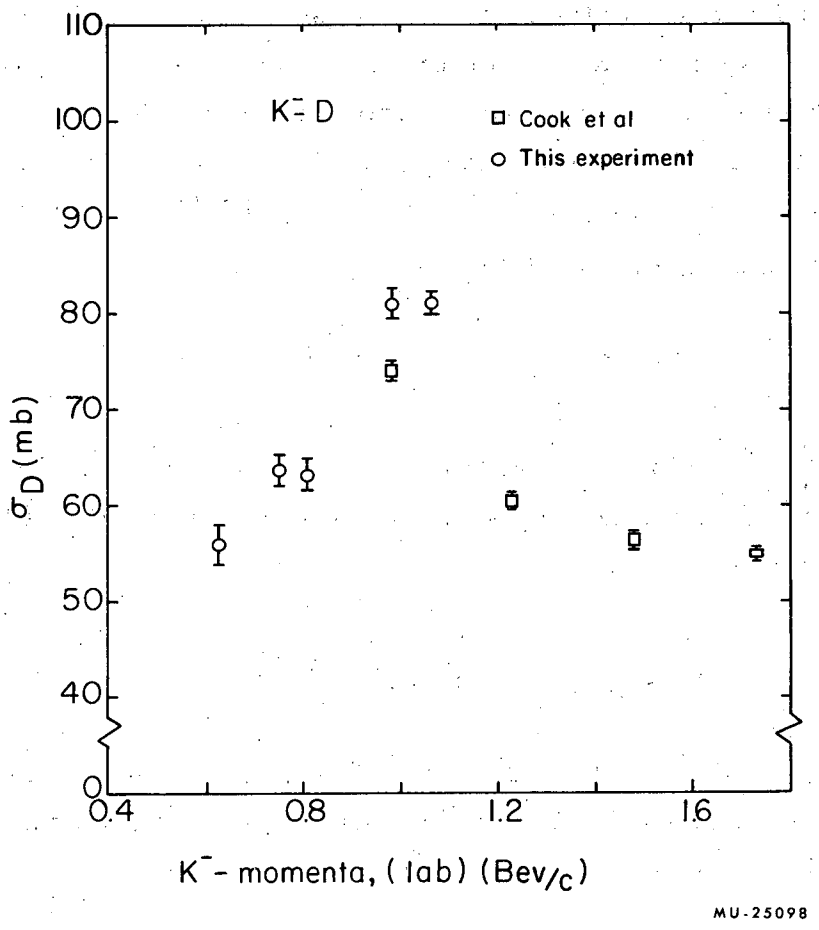

Fig. 16. The K^--d total cross sections plotted together with some of the data from the experiment of Cook et al.[5] We measured the K^--d cross sections at fewer points and with less statistical accuracy.

VIII. K^--NEUTRON TOTAL CROSS SECTIONS

The total cross section for collisions with deuterons has been found to be noticeably smaller than the sum of the corresponding cross sections for free neutrons and protons. Glauber formulated a theory for the cross sections in deuterium at high energies by taking into account the fact that either the neutron or the proton lies some of the time in the shadow cast by the other.[17] He gives the total cross section in deuterium (σ_d) in terms of the total cross sections on free neutrons (σ_n) and protons (σ_p) as

$$\sigma_d = \sigma_p + \sigma_n - (\sigma_p\ \sigma_n/4\pi)\left\langle \frac{1}{r^2} \right\rangle_d ,$$

where $\left\langle \frac{1}{r^2} \right\rangle_d$ is the mean inverse-square radius of the deuteron. Assuming that the deuteron has a radius of the order of the triplet effective range, we get

$$\left\langle \frac{1}{r^2} \right\rangle_d = \left(\frac{1}{1.7} \right)^2 (\text{fermi})^{-2}.$$

Typically, this correction amounted to about 10% of the difference $\sigma_d - \sigma_p$ (see Table XI). The K^--n total cross sections are plotted in Fig. 17.

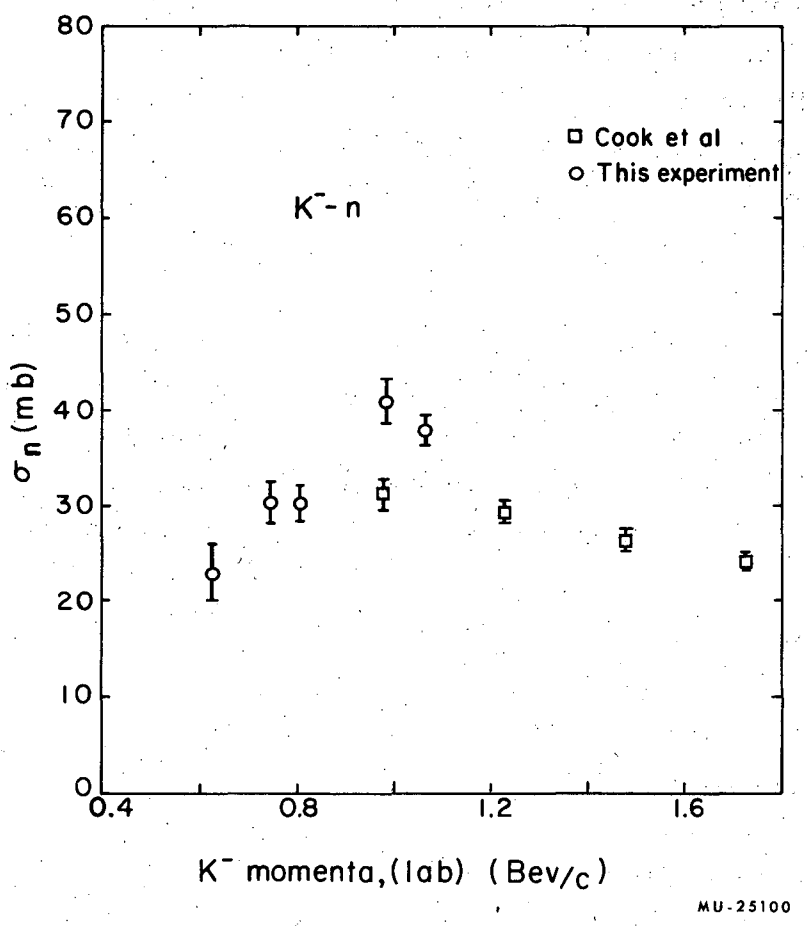

Fig. 17. The K^--n total cross sections obtained from hydrogen and deuterium data by applying Glauber's correction.[17]

IX. UNCERTAINTIES IN THE CALCULATED CROSS SECTIONS

The errors quoted in Tables X and XI include statistical errors, estimated errors in the calculated corrections, and error due to uncertainty in the atomic concentration of hydrogen or deuterium in the target. The counted data were divided into subgroups of 5000 K^- each, and the fluctuation amoung the subgroups was used to estimate the statistical part of the error. The hydrogen and deuterium data gave rms errors of about 23 and 20% respectively, higher than those estimated by using the total numbers, and assuming purely random count distributions.

Error in the forward scattering corrections is taken as 10% of the correction applied. Uncertainty in the decay-in-flight corrections can be estimated from the errors in the K^--decay branching ratios and the errors in the calculated probability integrals (see Section VIII-C). These errors were calculated and found negligible compared with the other error terms involved. The multiple Coulomb scattering corrections and light-particle contamination corrections also had uncertainties which were negligible compared with the statistical part of the error. The concentration n was calculated from our knowledge of the pressure and temperature of the liquids in the full target and the gas in the empty target. The operating pressure and temperature of the liquid hydrogen and deuterium was in general different during different runs. The length and the curvature of the end faces of the target flask were measured with high precision to calculate the effective length L of the target under different operating conditions. The factor $1/nL$ is presented in Table XII with the estimated uncertainties. The uncertainties in this factor, due to uncertainties in our knowledge of pressure, temperature, and length of the target, are also included in the quoted errors of the final cross sections (see Tables X and XI).

Apart from the random errors described in the preceding paragraph, a further systematic error of about 1 mb must be included. The cross sections deduced from the three counters T_1, T_2, and T_3 systematically disagreed by about this amount, the values decreasing

Table XII. Ratio $(1/nL)$, where n is the number of target nuclei per cm^3, and L is the length of target.

Nominal momenta (Mev/c)	1/nL (mb)
Hydrogen:	
700	400.2 ± 3.8
800	396.0 ± 2.1
900	397.0 ± 2.1
950	399.2 ± 3.8
1000	392.5 ± 1.7
1050	392.5 ± 1.7
1100	392.5 ± 1.7
1150	399.2 ± 3.8
1200	399.2 ± 3.8
Deuterium:	
700	335.2 ± 4.3
800	335.2 ± 4.3
900	333.0 ± 4.3
1050	335.2 ± 4.3
1150	335.2 ± 4.3

with the increasing size of counter. This effect is not completely understood, though part is certainly attributed to the fact that correction for forward scattering, which is proportional to counter size, is known to have been underestimated. Thus, in determining the cross section behavior from the results of Tables X and XI, the errors given may be legitimately used, but it should be borne in mind that the absolute normalization of the curve is uncertain by about 2 to 3% owing to systematic errors.

X. RESULTS

The total cross section results obtained in this experiment are presented in Tables X and XI, and these cross sections are plotted in Figs. 15 through 18, together with some high-energy data from counter experiments of Cook et al.[5] and some lower-energy data from the bubble chamber experiments of Bastian et al.[6]

As can be seen from Fig. 15, the agreement of the K^--p total cross section with the previous data is excellent. The K^--n data, however, do not agree to the same extent. There are no low-energy K^--n data available, and one can only compare with the data of Cook et al.[5] There seems to be a disagreement of approximately 8 mb in the overlapping region. This disagreement is not as bad as appears at first sight, when we remember that there can be an uncertainty of about 5% in the absolute normalization of the K^--n total cross sections obtained from this experiment, due to systematic errors in the K^--p and K^--d total cross sections. Similar uncertainties also exist in the cross sections from Cook et al., though of smaller magnitude. If we include the effect of the systematic errors, the K^--n cross section from the two experiments disagree by about 2 standard deviations, in the overlapping region.

XI. DISCUSSION OF RESULTS

The results from this experiment clearly show a large resonance-like peak in the K^--p total cross section (Fig. 15) at about 1050 Mev/c, with a width of approximately 200 Mev/c (full width at half-maximum). The peak also appears in the K^--d total cross section (Fig. 16). If we interpolate a smooth curve between the regions 600 to 700 Mev/c and 1200 to 1300 Mev/c, the peak in the K^--p cross section appears to extend about 15 mb above the nonresonant background value. The K^--n total cross sections (Fig. 17) seem to show a broader but lower peak at about the same momentum, but statistical inaccuracy does not allow us to decide whether such a peak really exists. Besides, the correction applied to arrive at the K^--n cross section from the K^--d cross section become less reliable when the K^--p cross section becomes large.

If we choose to call the observed peak in the K^--p total cross section a "resonance," it must have well-defined angular momentum, parity, and isotopic spin. The isotopic spin of the resonance can be deduced by assuming charge independence in the K-nucleon interaction. Therefore the interaction is completely specified by the two cross sections σ_0 and σ_1 corresponding to $I = 0$ and $I = 1$ states. The K^--n total cross section is pure $I = 1$ and the K^--p total cross section is composed of equal weights of $I = 0$ and $I = 1$: hence

$$\sigma_p = \frac{1}{2} (\sigma_0 + \sigma_1),$$

and

$$\sigma_n = \sigma_1 .$$

Thus any structure in the $I = 1$ state should be twice as evident in the K^--n as in the K^--p interaction, whereas interactions in the $I = 0$ state should appear only in the K^--p system. If the peak observed in the K^--p cross section were in the $I = 1$ state we should have observed a 30-mb peak in the K^--n cross section above the nonresonant background. Although there seems to be a broad peak in the K^--n total cross

section, it certainly is not strong enough to allow the K^--p resonance to be in the purely $I = 1$ state. Thus, the data are consistent with the interpretation that the resonance is largely in the $I = 0$ state. In discussing the possibility of a single-state $I = 0$ resonance at 1050 Mev/c, it should be kept in mind that this would still describe only part of the interaction at this energy, since there is a large nonresonant background of about 35 mb.

The maximum cross section at a resonance in the K^--nucleon system is $2\pi\lambda^2(2J + 1)$, where J is the total angular momentum, and λ is the de Broglie wavelength divided by 2π. At about the resonant energy (1050 Mev/c) we find that the most a $J = 1/2$ state can contribute is 17 mb. If this is confined to a single isotopic spin state, then the maximum contribution to the K^--p total cross section is 8.5 mb. The contribution from a $J = 3/2$ state is 34 mb; and if this is in the $I = 0$ state we can have a contribution of 17 mb in the K^--p cross section. Thus it seems necessary to attribute the resonance to a state of $J \geq 3/2$.

The resonance peak in the K^--p total cross section may be associated with the opening of new inelastic channels. At very low momenta the following reactions of K^- mesons on free protons are permitted by conservation of baryons, charge, and strangeness:

$$
\begin{aligned}
K^- + p &\rightarrow \Sigma^- + \pi^+ \\
&\rightarrow \Sigma^+ + \pi^- \\
&\rightarrow \Sigma^0 + \pi^0 \\
&\rightarrow \Lambda + \pi^0 \\
&\rightarrow \Lambda + 2\pi \\
&\rightarrow K^- + p \\
&\rightarrow \overline{K}^0 + n .
\end{aligned}
$$

As the K^- momentum is increased, inelastic channels for pion production open up. At about 1050 Mev/c K^- momenta, at least two new thresholds have been observed. One reaction, $K^- + N \rightarrow K + \Xi^-$, observed at 1.17 Bev/c[18], has a cross section of about 40 μb, and seems very unlikely to have an appreciable effect on the K^--p total cross section at 1050 Mev/c. The other recently discovered reaction, $K^- + p \rightarrow K^{*-} + p$,[19] has a threshold almost exactly at the resonant energy. The excitation function for this process is not known, but K^{*-} production at 1.15 Bev/c amounts to only a few mb. Other possible strong reactions at about this energy can be written down which involve higher excited-hyperon resonances analogous to the Y^*,[20, 21] aside from reactions that involve production of multiple pions.

At present, dispersion-relation techniques have been most successful in correlating and parameterizing the K-nucleon scattering data.[1, 22] Recently Ball and Frazer have used a dispersion theoretical approach to find a possible explanation of the higher pion-nucleon and K^--p resonances in terms of inelastic thresholds.[23] They have shown how a rapid rise in inelastic absorption in a given state (e.g., close to a threshold) can generate a large increase in the elastic scattering arising from the same state. From their dispersion relations between the real and imaginary parts of the phase shift in a given state, they show that, even for an inelastic cross section of only a few mb, the elastic cross section in the same state can be induced to rise to the unitarity limit. The peak in the total cross section should therefore occur close to the inelastic threshold. If this is the mechanism involved in the present case, it is susceptible to a direct experimental test, because the elastic and inelastic channels could be clearly associated as occurring with the same quantum numbers. By assuming the K^* has $J = 1$ and $I = 1/2$, Ball and Frazer found that the peaking in the cross section in the K^--p system should be five times as great as in the K^--n system.[23] The Fermi momentum of the neutron in the deuteron causes a broadening of the peak. If one assumes a

projected deuteron momentum of the order of 50 Mev/c, the half width should be increased by about 20%. Even though the present data on the K^--n total cross section (Fig. 17) do show a reduced and broadened peak, in agreement with the prediction of Ball and Frazer,[23] lack of sufficient statistical accuracy does not allow us to decide whether such a resonance actually exists or not.

Another interesting way to look at this resonance is from the point of view of the global symmetry hypothesis of Gell-Mann[24] and Schwinger.[25] It has been pointed out that from global symmetry, one would expect the same isobaric states that appear in the π-nucleon system to appear in the π-hyperon system.[21] Alston et al. have also pointed out that the (3, 3) resonance in the π-nucleon system under the foregoing assumption predicts a resonance in the π-hyperon system which corresponds to the mass of the Y^*.[20] The Y^* is below threshold in the K^-+p system. However, the other two isobaric states in the π-nucleon system predict isobaric states in the π-hyperon system above the threshold of the K^--nucleon system. In particular, the third resonance in the π-p system in the $I = 1/2$ state (total energy in the c.m. system equal to 1670 Mev) leads to a prediction of two resonances in the K^--nucleon system with $I = 0$ and $I = 1$, both in the region of 300 Mev in the c.m. system.[21] The resonance observed in the K^--p system is at slightly higher energy and is somewhat wider than would be expected from the π-nucleon resonance. However, such discrepancies need not imply complete disagreement with the idea of global symmetry, in view of the approximate nature of the scheme.

At present, the development of the theory of K-nucleon interaction is at a quite early stage. A complete theoretical interpretation of the behavior of the cross sections is therefore not possible. Further experimental information on both elastic and inelastic scattering processes will be necessary before one can definitely assign the cause of the observed resonance.

ACKNOWLEDGMENTS

It is my pleasure to thank Professor Kenneth M. Crowe for his interest and active participation in this experiment and for his patient guidance throughout my graduate research work. I would also like to take this opportunity to thank the many people without whose help and participation this experiment would have been impossible. I would like especially to thank Professor Owen Chamberlain, Professor Leroy T. Kerth, Professor Aaron Lemonick, Dr. Denis Keefe, and Dr. Theodor F. Zipf for their participation in the experiment and valuable advice during the analysis of the data.

The Bevatron crew under the direction of Dr. Edward J. Lofgren provided many hours of steady beam. For assistance in setting up and running the experiment, I would like to thank Dr. Carl M. York, Dr. Shinjiro Yasumi, Mr. Fred Betz, Mr. Helmut Dost, Mr. David Linn, Mr. Robert E. Shafer, and Mr. Wladyslaw Troka.

This work was performed under the auspices of the U. S. Atomic Energy Commission.

APPENDICES

A. Raw Data Tables

Table A-I. K^- - hydrogen data.

Nominal momenta (Mev/c)	No. of K^- mesons	Counts in transmission counters						Target
		T_1	$T_{1\,acc}$	T_2	$T_{2\,acc}$	T_3	$T_{3\,acc}$	
700	27 000	-	-	19 131	894	19 859	1 822	empty
700	32 506	-	-	20 897	1 138	21 878	2 377	full
800	36 031	-	-	26 856	1 188	27 938	2 799	empty
800	43 002	-	-	29 076	1 183	30 425	2 579	full
900	64 992	49 055	4 122	50 348	3 774	53 145	7 313	empty
900	81 413	55 693	5 252	57 637	4 691	61 700	9 255	full
950	39 003	29 983	2 928	30 716	2 878	32 234	5 583	empty
950	44 132	30 477	3 023	31 323	2 970	33 351	5 816	full
1000	62 404	47 621	2 930	48 617	2 691	51 847	6 398	empty
1000	71 006	48 452	3 192	49 573	2 891	53 693	7 311	full
1050	40 937	31 843	1 749	32 671	1 885	33 914	3 234	empty
1050	53 040	36 781	1 759	37 787	1 899	39 783	3 207	full
1100	55 823	43 573	2 329	44 630	2 122	46 956	4 828	empty
1100	61 000	42 153	2 175	43 339	2 174	46 298	4 815	full
1150	45 000	36 125	2 942	36 815	2 930	38 360	5 704	empty
1150	51 000	36 232	3 189	37 118	2 995	39 412	6 258	full
1200	61 521	47 767	2 624	49 352	2 853	51 355	4 991	empty
1200	86 045	59 954	3 136	62 060	3 657	65 435	6 229	full

Table A-II. K^--deuterium data.

Nominal momenta (Mev/c)	No. of K^- mesons	Counts in transmission counters						Target
		T_1	$T_{1\,acc}$	T_2	$T_{2\,acc}$	T_3	$T_{3\,acc}$	
700	16 980	11 552	478	11 826	583	12 338	1 095	empty
700	24 854	14 038	674	14 481	809	15 349	1 447	full
800	25 001	18 397	891	18 779	1 256	19 512	2 052	empty
800	35 000	21 094	1 086	21 668	1 441	22 913	2 477	full
900	29 753	22 014	1 655	22 674	1 643	23 847	3 023	empty
900	36 733	22 457	1 688	23 314	1 954	25 131	3 509	full
1050	32 003	25 159	2 093	25 715	1 863	26 837	3 961	empty
1050	42 853	26 690	2 107	27 541	2 117	29 708	4 354	full
1150	80 936	64 861	4 188	66 122	3 777	69 001	8 218	empty
1150	104 002	66 086	4 640	67 955	4 428	72 806	9 620	full

B. Decay-in-flight Corrections

1. First-Order Corrections

For corrections to the first order, we assume that all decay products miss the transmission counters. If, when the target is empty, N_{EO} K^- mesons pass the last Cerenkov counter C_2, the number that will survive at the transmission counter is given by

$$N_E = N_{E0} \exp[-x_2/\lambda] \exp[-\Sigma], \qquad \text{(B-1)}$$

where x_2 = the distance from a point midway between C_2 and B_4 to the transmission counter (see schematic below); and

λ = mean decay length of the K^- mesons,

Σ = attenuation factor due to the target assembly.

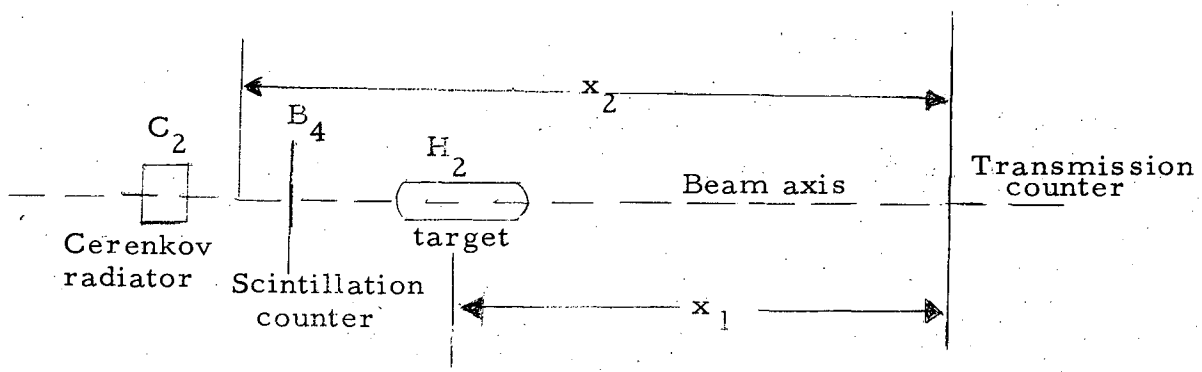

Fig. 18.

Similarly, when the target is full, we have the number of K^- mesons that will survive at the transmission counter given by

$$N_F = N_{F0} \exp[-n\sigma L] \exp[-\Sigma] \exp -[(x_2 - x_1)/\lambda] \exp[-x_1/\lambda'], \tag{B-2}$$

where

n = number of target nuclei per cm^3,

σ = length of target,

x_1 = distance between center of target and the transmission counter,

and

λ' = mean decay length of K^- mesons at the slightly reduced momentum after passing through the target.

The mean decay length is given by

$$\lambda = c\beta\gamma\tau = \frac{\tau}{m_0} p, \tag{B-3}$$

where quantities c, β, and γ have their usual meanings, τ is the mean life, p is the momentum, and m_0 is the rest mass of K^- mesons. From (B-3) we get, by substituting $m_0 = 494.0$ Mev and $\tau = 1.224 \times 10^{-8}$ sec,

$$\lambda = 24.37\ p, \tag{B-4}$$

where λ is in ft and p is in Bev/c.
Also from (B-3) we obtain

$$\frac{\Delta\lambda}{\lambda} = \frac{\Delta p}{p}. \tag{B-5}$$

If we write

$$\lambda' = \lambda - \Delta\lambda = \lambda\left(1 - \frac{\Delta\lambda}{\lambda}\right),$$

or

$$\lambda' = 24.37\ p\ \left(1 - \frac{\Delta p}{p}\right), \tag{B-6}$$

where Δp is the momentum loss in the target, the last exponential in Eq. (B-2) becomes

$$\begin{aligned}\exp[-x_1/\lambda'] &= \exp[-x_1/\lambda(1-\Delta\lambda/\lambda)], \\ &= \exp[-x_1/\lambda(1+\Delta\lambda/\lambda)], \\ &= \exp[-x_1/\lambda]\ \exp[(-x_1/\lambda)(\Delta\lambda/\lambda)], \\ &= \exp[-x_1/\lambda]\ \left(1 - \frac{x_1}{24.37}\ \frac{\Delta p}{p^2}\right). \qquad \text{(B-7)}\end{aligned}$$

Equation (B-2) therefore becomes

$$N_F = N_{F0}\ \exp[-n\sigma L]\ \exp[-\Sigma]\ \exp[-x_2/\lambda]\ \left(1-\frac{x_1}{24.37}\ \frac{\Delta p}{p^2}\right). \qquad \text{(B-8)}$$

From (B-1) and (B-8), the ratio of the target-empty and target-full transmission factors is given by

$$\frac{N_E/N_{E0}}{N_F/N_{F0}} = \exp[n\sigma L]\ \left(1 - \frac{x_1}{24.37}\ \frac{\Delta p}{p^2}\right)^{-1}.$$

The total cross section with the first-order correction is, therefore,

$$\sigma = \frac{1}{nL}\ \ell n\ \frac{N_E/N_{E0}}{N_F/N_{F0}} + \frac{1}{nL}\ \ell n\ \left(1 - \frac{x_1}{24.37}\ \frac{\Delta p}{p^2}\right),$$

or

$$\sigma_{1st} = \sigma_{uncorrected} - \frac{1}{nL}\ \left(\frac{x_1}{24.37}\ \frac{\Delta p}{p^2}\right). \qquad \text{(B-9)}$$

2. Complete Decay-in-Flight Corrections

If we take account of the probablity of charged decay products being counted in the transmission counter as K^- mesons, Eq. (B-1) becomes

$$\frac{N_E}{N_{ED}} = \exp[-x_2/\lambda]\,\exp[-\Sigma]+\int_0^{x_2-x_1}\exp[-\Sigma']\exp[-x/\lambda]\frac{dx}{\lambda}\sum_i B_i P_i\left\langle\theta(x)\right\rangle + \int_{x_2-x_1}^{x_2}\exp[-\Sigma]\,\exp[-x/\lambda']\,\frac{dx}{\lambda'}\sum_i B_i\,P_i'\,\left\langle\theta'(x)\right\rangle, \qquad \text{(B-10)}$$

where

B_i = K^- mesons decay branching ratio in the ith decay mode,

$P_i\left\langle\theta(x)\right\rangle$ = probability of detecting the decay products from the ith decay mode within an angle $\theta(x)$ about the direction of motion of the K^- mesons,

Σ' = attenuation factor for the decay products by the empty target assembly. The first term on the right-hand side of Eq. (B-10) represents the attenuation of K^- mesons due to decay in flight and the presence of the empty target assembly, the second term represents the probability of detecting decay products in the transmission counter from K^- decays ahead of the target, and the last term represents the probability of detecting decay products from K^- decays between the target and the transmission counter.

If we assume that the empty target assembly attenuates the decay products by the same factor as the K^- mesons (a good assumption) we have $\Sigma = \Sigma'$. Also, the momentum loss by the K^- mesons in passing through the empty target may be neglected. Thus $\lambda = \lambda'$. Hence Eq. (B-10) reduces to

$$\frac{N_E}{N_{E0}} = \exp[-x_2/\lambda]\exp[-\Sigma]+\frac{I}{\lambda}\exp[-\Sigma]\sum_i B_i\int_0^{x_2}\exp[-x/\lambda]\;P_i\left\langle\theta(x)\right\rangle dx. \qquad \text{(B-11)}$$

When the target is full, the momentum loss in the target is not negligible; hence the transmission factor for the full target is

$$\frac{N_F}{N_{F0}} = \exp[-(x_2-x_1)/\lambda]\ \exp[-x_1/\lambda']\ \exp[-\Sigma]\ \exp[-n\sigma L]$$
$$+ \frac{1}{\lambda}\exp[-\Sigma]\sum_i B_i \int_0^{x_2-x_1} \exp[-x/\lambda]\ P_i\langle\theta(x)\rangle\, dx$$
$$+ \frac{1}{\lambda'}\exp[-\Sigma]\ \exp[-n\sigma L]\sum_i B_i \int_{x_2-x_1}^{x_2} \exp[-x/\lambda']\ P_i'\langle\theta'(x)\rangle\, dx. \qquad \text{(B-12)}$$

Here again the respective terms represent the same quantities as in Eq. (B-10), except that the attenuation due to liquid hydrogen or deuterium is present in the first and the last terms.

The branching ratios of K^- mesons have been measured by N. A. Nickols[26] and were found to be consistent with the CPT theorem; that is, the agreement with the K^+-meson branching ratios was remarkably good. Therefore, in calculating decay-in-flight correction, the K^+ branching ratios[27] were used as they were statistically more accurate.

The probability $P_i\langle\theta(x)\rangle$ that a particle will decay into a cone of half-angle $\theta(x)$ can be written down exactly from our knowledge of the kinematics of the decay process. It is quite straightforward for the two most abundant decay modes $K_{\mu 2}$ and $K_{\pi 2}$. For three-body decay $P_i\langle\theta(x)\rangle$ is more complicated, but simplified calculations are possible, as shown by Blaton[13] and Baldin et al.[14] Hence all the integrals in Eq. (B-11) and (B-12) can be calculated, and an exact correction for the decay in flight may be made.

C. Multiple Coulomb Scattering and Beam Divergence Corrections

The horizontal beam profile F(r), as a function of distance from the beam axis, is shown in Fig. 14. The vertical profile is very similar to the horizontal. If we assume a cylindrically symmetric beam distribution about the beam axis, the number of particles passing through an element of area dA is

$$dN = F(r)\, dA = 2\pi r F(r)\, dr . \qquad (C-1)$$

The total number of particles in the beam is

$$N_0 = 2\pi \int_0^\infty r\, F(r)\, dr . \qquad (C-2)$$

A general method for applying the correction for multiple Coulomb scattering to experiments of this type is described by R. M. Sternheimer.[15] Barkas and Rosenfeld give a more accurate expression for this correction.[16] The general method is to assume that Coulomb scattering has a Gaussian distribution in angle, with a root-mean-square angle θ_{rms} given by

$$\theta_{rms} = \frac{15(\text{Mev})}{pv(\text{Mev})} \sqrt{L/L_{rad}}\, (1 + \epsilon) \text{ radians}, \qquad (C-3)$$

when p and v are the momentum and velocity of the particles respectively, and L/L_{rad} is the thickness of the scatterer in radiation lengths. The correction factor ϵ is given by Barkas and Rosenfeld.[16] Let us denote the Gaussian distributions due to multiple scattering in liquid hydrogen or deuterium by G(r): therefore,

$$\int_{-\infty}^{\infty} G(r)\, dr = 1 . \qquad (C-4)$$

If we have a circular counter of radius R, the number of particles passing through the counter when the target is empty is

$$N_E = 2\pi \int_0^R r\, F(r)\, dr\,. \qquad \text{(C-5)}$$

When the target is full, the number of particles passing through the counter is reduced because of multiple scattering, and is given by

$$N_F = 2\pi \int_0^R \int_{-\infty}^{\infty} r'\, F(r')\, G(r-r')\, dr\, dr'. \qquad \text{(C-6)}$$

Since all the functions involved in the integral of Eq. (C-6) are either measured or known, the integration can in principle be carried out exactly. In our case, the nature of the functions involved allows us to perform the integration in a much easier way. Let us write $2\pi\, r'\, F(r') = H(r')$ and note that $H(r')$ is a smoothly varying function with respect to $G(r - r')$. This allows us to expand $H(r')$ as

$$H(r') = H(r) + (r - r')\left[\frac{\partial H}{\partial r'}\right]_r + \frac{(r - r')^2}{2}\left[\frac{\partial^2 H}{\partial r'^2}\right]_r + \cdots \qquad \text{(C-7)}$$

Equation (C-6) therefore becomes

$$N_F = \int_0^R \int_{-\infty}^{\infty} G(r - r') \left\{ H(r) + (r - r')\left[\frac{\partial H}{\partial r'}\right]_r + \frac{(r - r')^2}{2}\left[\frac{\partial^2 H}{\partial r'^2}\right]_r + \cdots \right\} dr'\, dr, \qquad \text{(C-8)}$$

or

$$N_F = \int_0^R H(r)\, dr \int_{-\infty}^{\infty} G(r - r')\, dr'$$
$$+ \int_0^R \left[\frac{\partial H}{\partial r'}\right]_r dr \int_{-\infty}^{\infty} (r - r')\, G(r - r')\, dr'$$
$$+ \int_0^R \left[\frac{d^2 H}{dr'^2}\right]_r dr \int_{-\infty}^{\infty} \frac{(r - r')^2}{2}\, G(r - r')\, dr' + \cdots \qquad (C-9)$$

The second integral vanishes, since

$$\int_{-\infty}^{\infty} (r - r')\, G(r - r')\, dr' = 0.$$

Also we have

$$\int_{-\infty}^{\infty} (r - r')^2\, G(r - r')\, dr' = r_m^2,$$

where r_m is the projected mean radius due to multiple Coulomb scattering, at the location of the transmission counters. Hence Eq. (C-9) becomes

$$N_F = N_E + \frac{r_m^2}{2} \left[\frac{dH}{dr}\right]_R + \text{higher-order terms.} \qquad (C-10)$$

Probability of scattering into the transmission counter is

$$P(R) = \frac{N_F}{N_E} = \frac{N_E + r_m^2/2\,[dH/dr]_R}{N_E}. \qquad (C-11)$$

If we denote measured transmission factors by T_E and T_F for the empty and full target respectively, we can obtain the corrected cross sections:

$$\sigma_{corrected} = \frac{1}{nL} \ell n \frac{T_E}{T_F} P(R)$$

$$= \frac{1}{nL} \ell n \frac{T_E}{T_F} + \frac{1}{nL} \ell n \left(1 + \frac{r_m^2}{2N_E} \left[\frac{dH}{dr}\right]_R\right). \qquad (C\text{-}12)$$

Expanding the second log term we get, since $-1 < \frac{r_m^2}{2N_E} \left[\frac{dH}{dr}\right]_R < 1$,

$$\sigma_{corrected} = \sigma_{uncorrected} + \frac{1}{nL} \frac{r_m^2}{2N_E} \left[\frac{dH}{dr}\right]_R . \qquad (C\text{-}13)$$

The $[dH/dr]_R$ is a negative quantity, hence the correction decreases the magnitude of the measured cross section. The quantity r_m can be calculated from the known information about the target material, the particle momentum, and the distance of the transmission counter from the target. Terms N_E and $[dH/dr]_R$ are obtained from the measured beam profile. Thus the correction due to multiple Coulomb scattering can be applied without performing cumbersone integrations.

It should be noted that from a measurement of the horizontal and vertical beam scans a total of four H(r) are obtained. Since in the above calculation we assumed a cylindrically symmetric beam distribution, the corrections should be carried out for all four H(r) distributions. An average of the four corrections should be taken as the final correction. For a beam distribution that is not so uniformly distributed about the beam axis, more than two beam profiles will be necessary to obtain a good estimate of the correction by this method.

REFERENCES

1. For a recent compilation of data and references see L. T. Kerth, Revs. Modern Phys. 33, 389 (1961).
2. T. F. Kycia, L. T. Kerth, and R. G. Beander, Phys. Rev. 118, 553 (1960).
3. S. C. Freden, F. C. Gilbert and R. S. White, Phys. Rev. 118, 564 (1960).
4. G. von Dardel, D. H. Frish, R. Mermod, R. H. Milburn, P. A. Piroué, M. Vivargent, G. Weber, and K. Winter, Proceedings of the 1960 Annual International Conference on High-Energy Physics at Rochester (Interscience Publishers, Inc., New York, 1960). No. 10, p. 484.
5. V. Cook, B. Cork, T. F. Hoang, D. Keefe, L. T. Kerth, W. A. Wenzel and T. F. Zipf, Phys. Rev. 123, 320 (1961).
6. P. Bastien, J. P. Berge, O. Dahl, M. Ferro-Luzzi, W. E. Humphrey, J. Kirz, D. H. Miller, J. J. Murray, A. H. Rosenfeld, M. Ross, J. A. Schwartz, F. Solmitz, R. D. Tripp, M. Watson (unpublished). Preliminary data from this group have been reported by M. Ferro-Luzzi, Revs. Modern Phys. 33, 413 (1961).
7. L. W. Alvarez, Ninth Annual International Conference on High-Energy Physics Kiev, 1959 (Academy of Sciences, Moscow, 1960), p. 471.
8. R. H. Dalitz and S. F. Tuan, Ann. Phys. 8, 100 (1959).
9. C. Wiegand, I.R.E. Trans. on Nuclear Science NS-5, 77 (1958).
10. W. A. Wenzel, University of California Radiation Laboratory Report UCRL-8000, Oct. 2, 1957 (unpublished). Also see, Lawrence Radiation Laboratory Counting Handbook, University of California Radiation Laboratory Report UCRL-3307 Rev, Jan. 1, 1959 (unpublished).
11. R. L. Garwin, Rev. Sci. Instr. 24, 618 (1953).
12. E. Feenberg, Phys. Rev. 40, 40 (1932).

13. J. Blaton, Kgl. Danske Videnskab. Selskab, Mat.-Fys. Medd. Bind XXIV, Nr. 20, p. 6.
14. A. M. Baldin, V. I. Goldanskii and I. L. Rozenthal, Kinematics of Nuclear Reactions (Pergamon Press, New York, 1961).
15. R. M. Sternheimer, Rev. Sci. Instr. 25, 1070 (1954).
16. W. H. Barkas and A. H. Rosenfeld, Data for Elementary-Particle Physics, Lawrence Radiation Laboratory Report UCRL-8030-Rev, Oct. 1, 1961 (unpublished).
17. R. J. Glauber, Phys. Rev. 100, 242 (1955); Also see Nuclear Forces and Few Nucleon Problems, Vol. I, edited by T. C. Griffith and E. A. Powers (Pergamon Press, New York, 1960).
18. W. B. Fowler, R. W. Birge, P. Eberhard, R. Ely, M. L. Good, W. M. Powell, and H. K. Ticho, Phys. Rev. Letters 6, 134 (1961).
19. M. Alston, L. Alvarez, P. Eberhard, M. L. Good, W. Graziano, H. K. Ticho, and S. Wojcicki, Phys. Rev. Letters 6, 300 (1961).
20. M. Alston, L. Alvarez, P. Eberhard, W. Graziano, M. L. Good, H. K. Ticho, and S. Wojcicki, Phys. Rev. Letters 5, 520 (1960).
21. L. T. Kerth and A. Pais, On the Gentle Art of Hunting Bumps in the Pion-Hyperon System, Lawrence Radiation Laboratory Report UCRL-9706, May 1961 (unpublished).
22. R. H. Dalitz, Rev. Modern Phys. 33, 471 (1961).
23. J. S. Ball and W. R. Frazer, Phys. Rev. Letters 7, 204 (1961).
24. M. Gell-Mann, Phys. Rev. 106, 1296 (1957).
25. J. Schwinger, Ann. Phys. 2, 407 (1957).
26. N. A. Nickols, The Lifetime and Decay Modes of Negative K Mesons (Ph. D. Thesis), Lawrence Radiation Laboratory Report UCRL-8692, Sept. 1959 (unpublished).
27. R. W. Birge, D. H. Perkins, J. R. Peterson, D. H. Stork, and M. N. Whitehead, Nuovo cimento 4, 834 (1956)., G. Alexander, R. H. W. Johnston, and C. O'Ceallaight, Nuovo cimento 6, 478 (1957).
28. G. Frye and R. L. Warnock, Bull. Am. Phys. Soc. 1, 56 (1962).

29. Wang Yung and Hu Shih-ko, On Resonances in Elastic K Meson-Nucleon Scattering, U. S. S. R. Report No. D-633, (Joint Institute for Nuclear Research, Dubna, 1960).
30. William E. Humphrey, Hyperon Production by K^- Mesons Incident on Hydrogen (Thesis), Lawrence Radiation Laboratory Report UCRL-9752, June 1961 (unpublished).
31. Ulrich Kruse and Michael Nauenberg, S-Wave K^--N Scattering Amplitudes, Lawrence Radiation Laboratory Report UCRL-8888, September 11, 1959 (unpublished).
32. Paul Nordin, Jr., S- and P-wave Interactions of K^- Mesons in Hydrogen (Thesis), Lawrence Radiation Laboratory Report UCRL-9489, November 21, 1960 (unpublished).
33. R. H. Dalitz, K Mesons and Hyperons, Their Strong and Weak Interactions, in Reports on Progress in Physics, Vol. 20 (Institute of Physics and the Physical Society, London, 1957).
34. R. H. Dalitz, Theoretical Interpretation of Strange Particle Interactions in Proceedings of the 1958 Annual International Conference on High-Energy Physics at CERN, edited by B. Ferretti (CERN Scientific Information Service, Geneva, 1958).
35. D. Amati, N. Fierz and V. Glaser, Phys. Rev. Letters 4, 89 (1960).
36. S. F. Tuan, Nuovo cimento 18, 1301 (1960).